UPPSALA
UNIVERSITET

UPTEC E 21007
Examensarbete 30 hp
Juni 2021

Methods of self-interference cancellation in full duplex telecommunication systems

Henrik Erlandsson
Viktor Sköldheden

Civilingenjörsprogrammet i elektroteknik

UPPSALA
UNIVERSITET

Methods of self-interference cancellation in full duplex telecommunication systems

Henrik Erlandsson
Viktor Sköldheden

Abstract

With the wireless technology evolving quickly, so does the demand of speed and efficiency. This makes the companies look for new and better ways to improve the current systems. One way of improving the present systems would be to employ Full Duplex Technology. In recent years the standard has been Half duplex technology with either Time Division Duplexing (TDD) or Frequency Division Duplexing (FDD). The drawback of TDD is that the signals is put in different time slots, meaning if many signals is to be transmitted at the same time there will be a delay. For FDD the signals are sent at different frequencies. This takes up a lot of space in the spectral domain. Full Duplex Technology has the potential to double the spectral efficiency with it's power to transmit and receive signals simultaneously at the same frequency. The main challenge with Full Duplex (FD) is the leaking Self-Interference (SI) from the transmitter to the receiver. Different methods can be used to suppress the SI in both the digital and the analog domain. Typically the Self-Interference Cancellation (SIC) is split into three parts. The passive Radio Frequency (RF) SIC, which suppresses the signal using for example. antenna separation, antenna polarization or a circulator. The active analog RF cancellation which could for example use a multi-tap analog least mean square adaptive and finally the Digital passband SIC, that is addressed in this thesis. The cancellation in the RF domain needs to suppress enough for the Low Noise Amplifier (LNA) and the Analog to Digital Converter (ADC) to not saturate. The Digital SIC should optimally suppress the signal to the noise floor to be able to demodulate the received signal. In this thesis modelling and reconstruction of the SI signal has been done. An attempt to model the non-linearities from the Power Amplifier (PA), the imbalance from the IQ-mixer and the effects of the circulator has been done to as correctly as possible comply to the real signal distortions. Simulations using experimental data provided by Syntronic SRD was used to evaluate the cancellation for Recursive Least Square (RLS), Ordinary Least Square (OLS) and Normalized Least Mean Square (NLMS) algorithms. The simulations shows that a cancellation of over 45dB within the bandwidth can be achieved using digital cancellation in the baseband. The result shows the importance of having a weakly nonlinear transmit signal to achieve a better performance using FD. It was showed that the linear model shows significantly worse results in comparison to the Generalized Memory Polynomial (GMP) and Memory Polynomial (MP). The MP and GMP model achieve similar results in the weakly non-linear cases but the GMP outperforms the MP model in strongly non-linear cases.

Teknisk-naturvetenskapliga fakulteten

Uppsala universitet, Utgivningsort Uppsala/Visby

Handledare: Mahmoud Alizadeh Ämnesgranskare: Mikael Sternad

Examinator: Mikael Bergkvist

Foreword

This thesis was done at Syntronic SRD in Gävle, Sweden. The purpose of this thesis was to evaluate different methods and models for full duplex self-interference cancellation in the digital domain.
We would like to gratefully thank our school supervisor Professor Mikael Sternad for guiding us through this thesis. We would also like to thank our supervisor at Syntronic SRD, Mahmoud Alizadeh. For all the time and effort that he has put in to make this thesis possible and also for providing us with all the necessary measurement data. Finally would we like to thank Syntronic SRD for having us and letting us do our master thesis at their office.

Contents

Acronyms

ADC Analog to Digital Converter.

ALMS Analog Least Mean Square.

BER Bit Error Rate.

DAC Digital to Analog Converter.

DPD Digital Pre Distortion.

FD Full Duplex.

FDD Full Division Duplexing.

FFT Fast Fourier Transform.

GMP Generalized Memory Polynomial.

HD Half Duplex.

IFFT Inverse Fast Fourier Transform.

LNA Low noise Amplifier.

MP Memory Polynomial.

MSE Mean Square Error.

NLMS Normalized Least Mean Square.

OFDM Orthogonal Frequency Division Multiplexing.

OLS Ordinary Least Square.

PA Power Amplifier.

QAM Quadrature Amplitude Modulation.

RF Radio Frequency.

RLS Recursive Least Square.

SI Self-Interference.

SIC Self-Interference Cancellation.

SIR Signal to interference ratio.

SNR Signal to Noise Ratio.

TDD Time Division Duplexing.

VSG Vector Signal Generator.

1 Introduction

1.1 Introduction

The world is evolving and so are the system for wireless communication. Researchers try to find methods of implementing full duplex (FD) with various results. Nowadays, telecommunications systems uses half-duplex (HD) systems. These systems are either based on the frequency division duplexing (FDD) or the time division duplexing (TDD). Both those methods are used to avoid self interference. FD is a technique that transmits and receives data simultaneously at the same frequency.

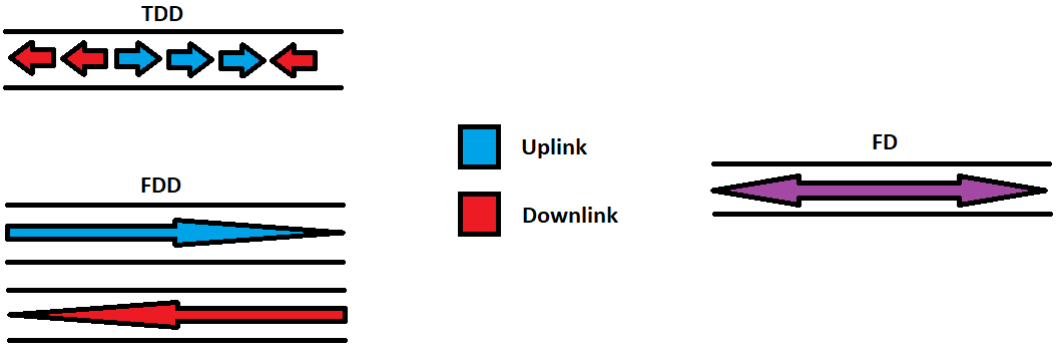

Figure 1.1: TDD,FDD and FD

As presented in figure 1.1 TDD transmits data over the same frequency in different time slots. FDD transmits simultaneously in time but at different frequencies and FD transmits simultaneously at the same frequency. FD wireless communication systems have the potential of doubling the spectral efficiency of existing HD systems. The most notable difference between FD and HD is the optimization in spectral efficiency. In FD you don't have to sacrifice any bandwidth or delay the signal in comparison to the half duplex systems. If the SIC were perfect an example of where you would use FD would be in WiFi. When you want to upload and download at the same time in HD, the downlink is prioritized and the uplink is put in a queue. This results in increased latency especially with multiple devices connected at the same time. The latency would be improved with the use of a FD system. [1] Also Full-duplex can work as a type of encryption. If someone tries to hack your system in a half-duplex system they receive the desired data. However in a full-duplex system the hacker would receive a combination of transmitted and received data which would be harder to decode.
The difficult part with FD is the self-interference (SI) that occurs with the transmitted signal being picked up by the receiver antenna. This basically means that the received signal is a combination of the transmitted signal and the received signal. As the transmitted signal is known, ideally this signal could be subtracted from the received signal. However the SI is not the same as the generated signal. This is because the signal is being processed through multiple devices that leads to signal manipulations. Both non-linearities, time shifts and phase shifts occur. To cancel out the SI-signal the transfer function for the system needs to be well approximated. The problem with wireless FD systems is that the self interference is millions to billions (60-90dB) times stronger than the received signal. There has been many researches in this topic that addresses different methods, models and limitations in full duplex [2] [3] [4] [5] to name a few.
The FD self-interference cancellation (SIC) can be divided into three parts. The radio frequency (RF) SIC which is cancelled in the RF-domain by for example isolating the transmitter and the receiver. The Analog SIC which also is done in the RF domain using analog techniques. Both the RF SIC and the analog SIC main purpose is to cancel enough for the low noise amplifier (LNA) and the analog to digital converter (ADC) to no saturate. The final cancellation is the Digital SIC which will be addressed further in this thesis, cancelling enough of the SI in the digital domain to be able to decode the received signal.

1.2 Project specifications and purpose

This thesis will focus on the digital cancellation in the FD system. A model will be constructed to estimate the properties of the SI signal, if the transmitted signal is known. Three different methods,

ordinary least square (OLS), normlized least mean square (NLMS) and recursive least square (RLS) will be tested in a simulation environment to adjust the model and to cancel out the self-interference from a received signal where the transmitted signal is known. This thesis was set up by Syntronic SRD. The purpose of the thesis was to test different methods and models in FD. The goal was to:

- find out how the level of non-linearity in the signal affect the SIC.
- Estimate the SINR compression using different methods.
- Estimate the SI impact on adjacent and alternate channels using OLS.

The performance of the different methods was evaluated using:

- Signal to Interference plus Noise Ratio (SINR).
- Signal to Noise Ratio (SNR).
- Bit Error Rate (BER).
- dB Compression

1.3 Outline

Chapter two explains the theory of the signal chain. Chapter three gives an explanation of how the modelling of the transfer function throughout the signal chain is estimated. Chapter four presents the different methods and models that are used to reconstruct the signal chain and chapter five presents the results and discussion.

1.4 Work distribution

All parts of the thesis has been thoroughly discussed and researched together. All parts of the simulations and theory have been done as a group. Below is an explanation of the sections that each individual has put more focus into in the report.

1.4.1 Henrik

The theory and model of the Orthogonal Frequency Division Multiplexing (OFDM) generation and demodulation using the 4 Quadrature Amplitude Modulation (4QAM) except the pilot, presented in section 2.1.2 and section 3.1.
The theory and the modelling of the IQ-mixer presented in section 2.3 and section 3.2.
The theory of the amplifiers presented in section 2.4.
The theory and modelling of the low pass filters presented in section 2.5 and section 3.5.
The OLS method and results presented in section 4.2 and section 5.1.1

1.4.2 Viktor

The reference signal in the OFDM generation in this thesis referred to as the pilot, presented in the end of section 2.1.2 and section 3.6.
The theory about the ADC and the Digital to Analog Converter (DAC) presented in section 2.2.
The theory and the modelling of the RF SIC presented in section 2.6.1 and section 3.4.
The theory of the analog SIC which is presented in chapter 2.7.
The modelling of the PA presented in section 3.3.
The NLMS and RLS methods presented in 4.1 and 4.3 with their respective results in section 5.1.2 and section 5.1.3.

2 Signal chain

The current systems are using half-duplex TDD or FDD where the received and transmitted signal is either sent and received at different time slots or sent at separate frequencies. When a receiver and a transmitter works simultaneously at the same frequency SI occurs. To counteract the SI, different cancellation techniques can be implemented. The simplified version of the transceiver (FD SI cancellation scheme from a generated signal to a received signal) is shown in figure 2.1. The cancellation can roughly be divided into three cancellation segments. *Passive RF*, *Analog RF* and *Digital baseband cancellation*. To achieve a working FD system the SI needs to be compressed down close to the noise floor [6]. However Quadrature phase-shift keying can achieve a very small BER if the signal has an SNR of at least 10dB according to [7].

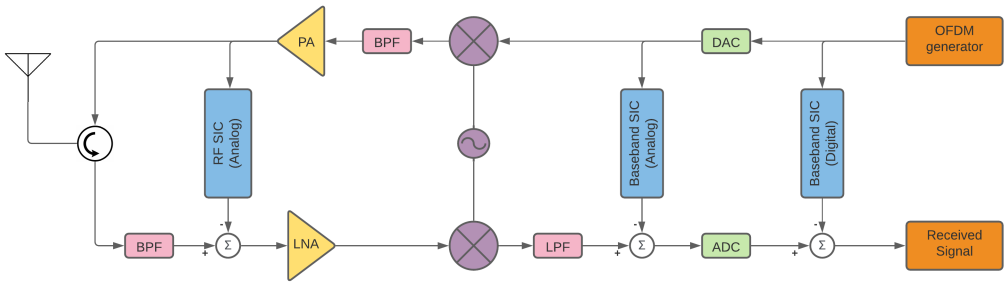

Figure 2.1: Block diagram of the simplified version of the signal chain

2.1 OFDM-signal generation and received signal

In figure 2.1 the simplified version of the signal chain is presented. Here, the signal is generated in the OFDM generator block. The signal is then converted from a digital to an analog signal in the DAC. the analog signal is then upconverted from baseband frequency to passband frequency in the purple block that represents the IQ-mixer.
The upconverted signal is then amplified in the yellow PA block representing the power amplifier. When the signal is amplified it enters the circulator represented by the round block with an arrow inside. The circulator is in this block diagram the RF passive SIC block. The circulator is present to block the transmitted signal from leaking into the receiver side of the signal chain. As the transmitted signal leaves the antenna another signal enters the antenna as a received signal from another transmitter (the signal we are after). However, as the transmitted signal enters the circulator, some of it also leaks into the receiver end together with the received signal. This means that in the receiver end of the signal chain (the bottom row in figure 2.1) consists of a signal with both the received signal as well as a leaked part of the transmitted signal, the SI. The combined signal, where the SI is much larger than the received signal is amplified in the LNA. After the combined signal has been amplified it is downconverted from passband to baseband (in the purple block representing the IQ-mixer) and finally converted from an analog to a digital signal (in the ADC block) before it is demodulated in the received signal block. With full duplex, when the signal in the receiver side of the signal chain being a combination of SI and the received signal, the SI needs to be cancelled out. This is done in the passive RF SIC block (the circulator mentioned before) as well ass all the blue blocks that represents different parts of the SIC. It is crucial that the passive and the active analog SIC (the cancellation the furthest to the left in figure 2.1) cancel enough such that neither the LNA nor the ADC is saturated, preventing loss of data.

2.1.1 MQAM

MQAM is a modulation which encodes bits in both amplitude and phase in M discrete complex-valued symbols. For example in 4QAM, 2 bits at the time are encoded as a complex number corresponding to the constellation diagram shown in Figure 2.2. As an example a bitstream of 6 bits $b = [110100]$, when encoded using 4QAM from Figure 2.2, would be 3 QAM symbols $x = [-1 - j, -1 + j, 1 + j]$

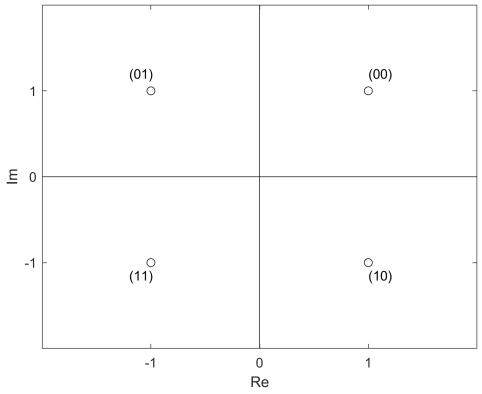

Figure 2.2: Constellation diagram of 4QAM

2.1.2 OFDM generation

Orthogonal Frequency-Division Multiplexing (OFDM) is a technique used to encode digital data on multiple baseband carrier frequencies. It is an efficient way of transmitting data as it both has a high data throughput, high spectral efficiency and a high data integrity. This is done by transmitting over thousands of overlapping but orthogonally spaced carriers simultaneously at a relatively slow symbol rate [8].

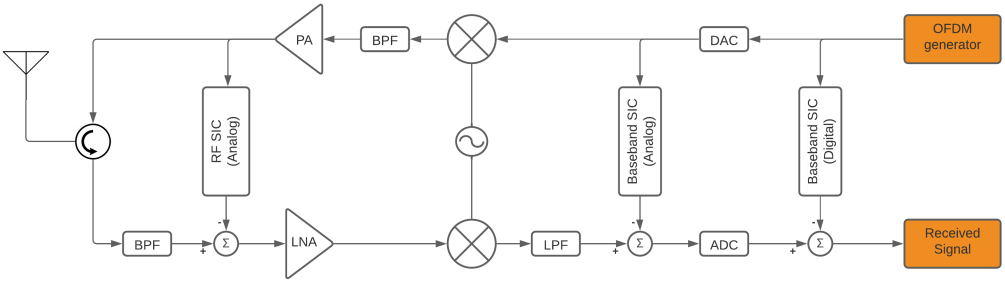

Figure 2.3: Block diagram of the simplified version of the transceiver, Signal modulator and demodulator highlighted.

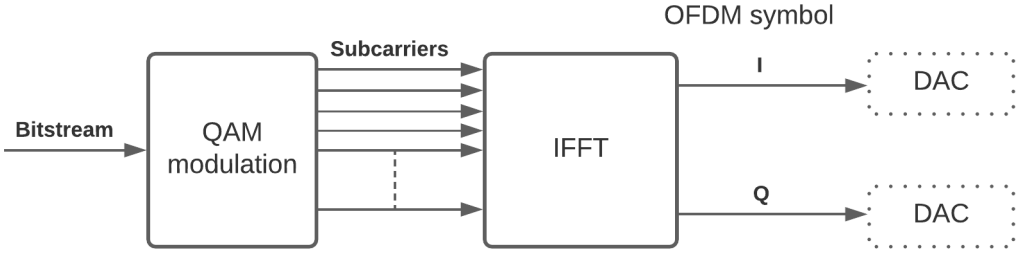

Figure 2.4: A basic representation of how OFDM symbols are generated from a bitstream

The generation of OFDM symbols are shown in Figure 2.4. The input bitstream is modulated using QAM, which will result in a stream of N symbols $X[0], X[1], ..., X[N-1]$. The N set of QAM symbols determine the amplitude and phase of the discrete frequency components at each subcarrier frequency of the OFDM symbol. These frequency components are converted to time samples using inverse fast Fourier transform (IFFT). The result of the IFFT is a complex valued baseband OFDM symbol x[n]=[x[0],x[1],...,x[N-1]]

with length N,defined by

$$x[n] = \frac{1}{\sqrt{N}} \sum_{i=0}^{N-1} X[i] e^{j2\pi ni/N} \tag{2.1}$$

Usually a cyclic prefix of length μ is added to the OFDM symbol to separate each OFDM symbol, which means the resulting time samples will be $x[n] = [x[N-\mu], ..., x[0], ..., x[N-1]$[9]. The time samples are then separated into a real and an imaginary part, $I = Re(x[n])$ and $Q = Im(x[n])$, which goes to the DAC. The DAC is described in section 2.2 below.

The received signal is phase shifted and attenuated, both from the transmitting circulator, the medium it passes through and the receiver circulator which can be seen in figure 2.1. To synchronize the signal back to its original phase a reference pilot is sent from the transmitter. This reference signal, in this thesis called a pilot is known by the receiver. There are several different ways of sending this pilot, also known as the Demodulation-Reference Signal (DM-RS) [10]. The DM-RS signal should preferably have the following properties.

- The signal should have small power variations in the frequency domain. The small variation gives a similar channel estimation over all frequencies in the reference signal.
- Limited power variations in the time domain, leading to a low Peak to average power ratio (PAPR) and a low cubic metric of the transmitted signal. [11]
- Furthermore, a sufficient number of reference-signal sequences of a given length, corresponding to a certain reference-signal bandwidth, should be available in order to avoid an unreasonable planning effort when assigning reference-signal sequences to devices and cells.[12]

After the signal is phase corrected the signal is transformed back into the array of subcarriers through a fast fourier transform (FFT). Each subcarrier is demodulated using QAM. Finally the signal is multiplexed to recreate the original data stream [13].

One way of generating an OFDM pilot with length N is by setting every other input symbol to 0. This implies $X[n] = 0, n = 1, 3, 5...$, if that symbol is plugged in to equation (2.1) it can be shown that it is periodic with period N/2.

$$x[n] = \frac{1}{\sqrt{N}} \sum_{i=0}^{N-1} X[i] e^{j2\pi ni/N} = \frac{1}{\sqrt{N}} \sum_{i=even} X[i] e^{j2\pi ni/N} \tag{2.2}$$

and

$$x[n + N/2] = \frac{1}{\sqrt{N}} \sum_{i=even} X[i] e^{j2\pi (n+N/2)i/N} = \frac{1}{\sqrt{N}} \sum_{i=even} X[i] e^{j2\pi ni/N} = x[n] \tag{2.3}$$

This implies that $x[n] = x[n + N/2]$
Since the pilot is periodic there will be correlation. This can be used to estimate where the signal starts. When the start of the signal is found, first the OFDM pilot is demodulated to input symbols. Since the input symbol $X[i] \neq 0$ is predefined this information can be used to estimate the channel over the whole bandwidth by comparing them with the received pilot. For example, if the received pilot is phase-shifted and amplified or attenuated as $A_i X[i] \angle \alpha_i$ then the gain $A_{i=even}$ and the phase $\alpha_{i=even}$ can be found since $X[i_{even}]$ is known. Then $A_{i=odd}$ and $\alpha_{i=odd}$ can be estimated with interpolation. When A_i and α_i are found these are an estimate of what the channel looks like. which means they can be used to "correct" the amplitude and phase of the other OFDM symbols containing data. A visual representation of the construction of a pilot can be is shown in figure 2.5, where the input symbols marked in yellow are the predefined input symbols in the pilot.

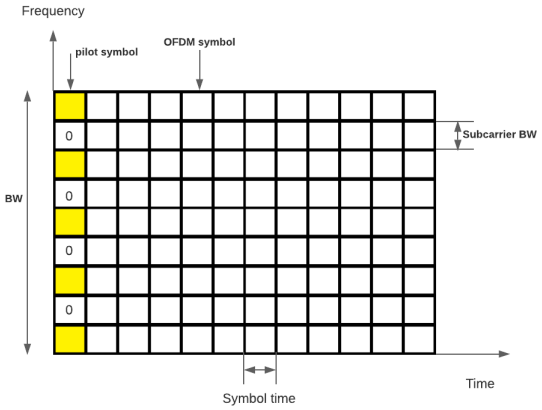

Figure 2.5: Visual representation of one OFDM pilot followed by OFDM symbols contain data

2.2 DAC/ADC

The DAC and the ADC can be found in the beginning respectively the end of the chain as seen in Figure 2.6. For QAM which is used in this thesis the DAC is converting the complex-valued digital baseband signal to two analog signals, one being in-phase and one being quadrature phase 90°phase shifted. The ADC doing the opposite, receiving two analog signals and converting them to a single digital complex-valued signal.

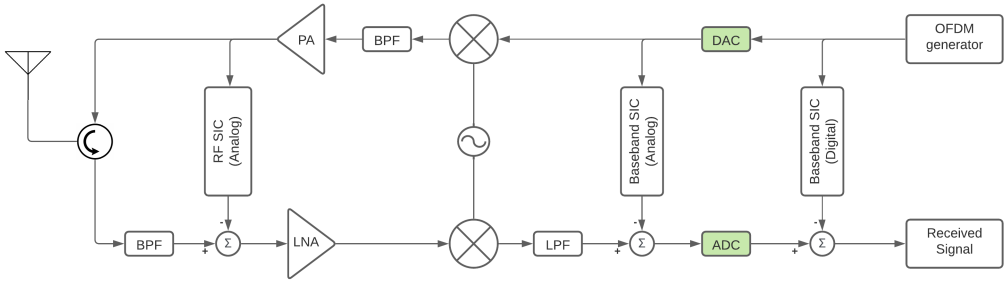

Figure 2.6: Block diagram of the simplified version of the transceiver, ADC and DAC highlighted.

The challenge converting the analog signal to a digital signal is if the ADC gets saturated. A saturation in the ADC means the resolution is not high enough leading to loss of data. If the signal is not attenuated enough in the analog domain the dynamic range of the ADC will be insufficient and the resolution of the signal will be very low [14]. The quantization noise from the ADC decreases the SINR, meaning the quantization noise floor needs to be high enough for the signal to be properly converted. The power of the quantization noise floor can be shown in equation (2.4).

$$P_{Quantization} = P_{AD_{total}} - SNR_{adc} \tag{2.4}$$

where $P_{AD_{total}}$ is the total power that enters the ADC and $SNR_{adc} = 6.02b + 1.76 - PAPR$ where PAPR is the peak to average power and b is the number of bits in the ADC. [15] Comparing $P_{Quantization}$ with $P_{received}$ gives a numerical value that expresses the decrease in the bit resolution as $P_{Quantization} \rightarrow P_{received}$.
This means that the signal achieved by the ADC is dependent on the analog cancellation. If the SINR is below a certain level the ADC is saturated and the signal loses data (low resolution). The number of bits used in the ADC decides the levels of SINR that is acceptable. Generally 12-bit, 16-bit, or 24-bit are used with more bits increasing the cost of the ADC. Therefore naturally the companies desires a lower number of bits to keep the cost down.
In this thesis the analog cancellation is assumed big enough, meaning there is no losses in the received signal. If this was not the case the digital cancellation would be impossible as a result of the desired

signal already being corrupt.

2.3 IQ-mixer

IQ Modulators mix baseband signal up to RF signals. Standard mixers uses three ports, the Local Oscillator port, the RF port and the Intermediate Frequency port. An IQ mixer uses two separate ports instead of the IF port, an in-phase port and a quadrature port. The IQ-mixer up- or down-converts the center frequency from baseband to passband or passband to baseband.

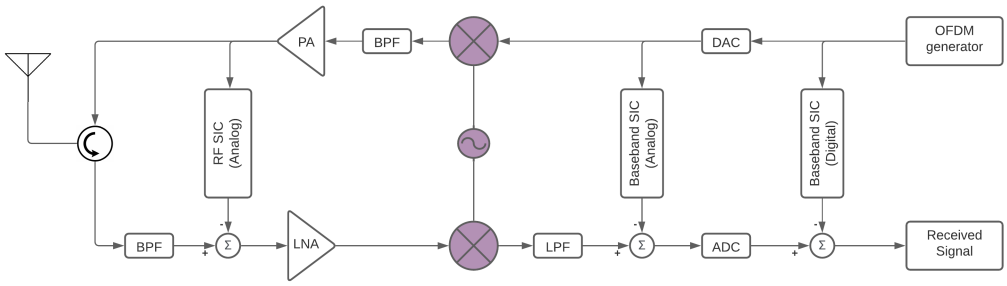

Figure 2.7: Block diagram of the simplified version of the transceiver, IQ-mixer highlighted

The mixer receives an in-phase and a quadrature signal from the DAC. These signals are described by equation (2.5) for in-phase and equation (2.6) for the quadrature-phase. The signals are upconverted using the LO to the desired transmission frequency. The signals are then decoded and downconverted by the IQ-mixer and LO. The phase adds for the upper sideband and subtracts for the lower sideband (180°out of phase) resulting in the I and Q signals with the desired in-band frequency.

$$In\text{-}Phase = Icos(2\pi ft) \tag{2.5}$$

$$Quadrature\text{-}phase = Qsin(2\pi ft) \tag{2.6}$$

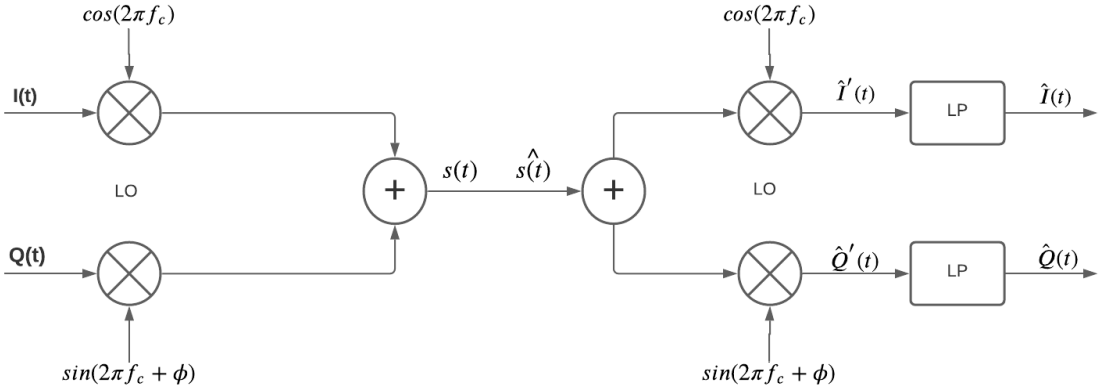

Figure 2.8: Block diagram of IQ mixer, both up conversion and down conversion

From Figure 2.8, the modulation of $I(t)$ and $Q(t)$ results in the transmitted signal

$$s(t) = I(t)cos(2\pi f_c) + Q(t)sin(2\pi f_c + \phi) \tag{2.7}$$

where f_c is the carrier frequency (or RF) and ϕ is the imbalance from the two LOs. If the IQ-mixer is ideal the phase between the in-phase and quadrature components would be 90°, which means $\phi = 0$.

Assume perfect transmission and no imbalance, $\hat{s}(t) = s(t)$ and $\phi = 0$, then in demodulation (or down conversion) the in-phase component

$$\begin{aligned}\hat{I}'(t) = \hat{s}(t)cos(2\pi f_c) &= (I(t)cos(2\pi f_c) + Q(t)sin(2\pi f_c))cos(2\pi f_c) \\ &= I(t)cos^2(2\pi f_c) + Q(t)sin(2\pi f_c)cos(2\pi f_c) \\ &= I(t)\frac{1}{2}(1 + cos(2\pi 2 f_c)) + Q(t)\frac{1}{2}sin(2\pi 2 f_c)\end{aligned} \tag{2.8}$$

It can be seen that to retrieve only the in-phase component $I(t)$ a lowpass filter can be used to filter out the components at frequency $2f_c$, which yields $\hat{I(t)} = LP(\hat{I}'(t)) = \frac{1}{2}I(t)$
A similar procedure is done to retrieve the quadrature component $Q(t)$, which yields $\hat{Q}(t) = LP(\hat{Q}'(t)) = \frac{1}{2}Q(t)$. However, in a real case there will be imbalances in both up and down conversion. This means that $\phi \neq 0$ and will have to be considered. By using the equation (2.8) with $\hat{s}(t)$ as in equation (2.7) with $\phi \neq 0$ it can be shown that

$$\begin{aligned}\hat{I}(t) = LP(\hat{I}'(t)) &= \frac{1}{2}(I(t)cos(\phi) + Q(t)sin(\phi)) \\ \hat{Q}(t) = LP(\hat{Q}'(t)) &= \frac{1}{2}(Q(t)cos(\phi) + I(t)sin(\phi))\end{aligned} \tag{2.9}$$

From equation (2.9) it can clearly be seen that the retrieved in-phase component $\hat{I}(t)$ not only contains the in-phase component $I(t)$ but also the quadrature component $Q(t)$ depending on the imbalance ϕ. And also that the quadrature component $\hat{Q}(t)$ contains both $I(t)$ and $Q(t)$, also depending on ϕ.

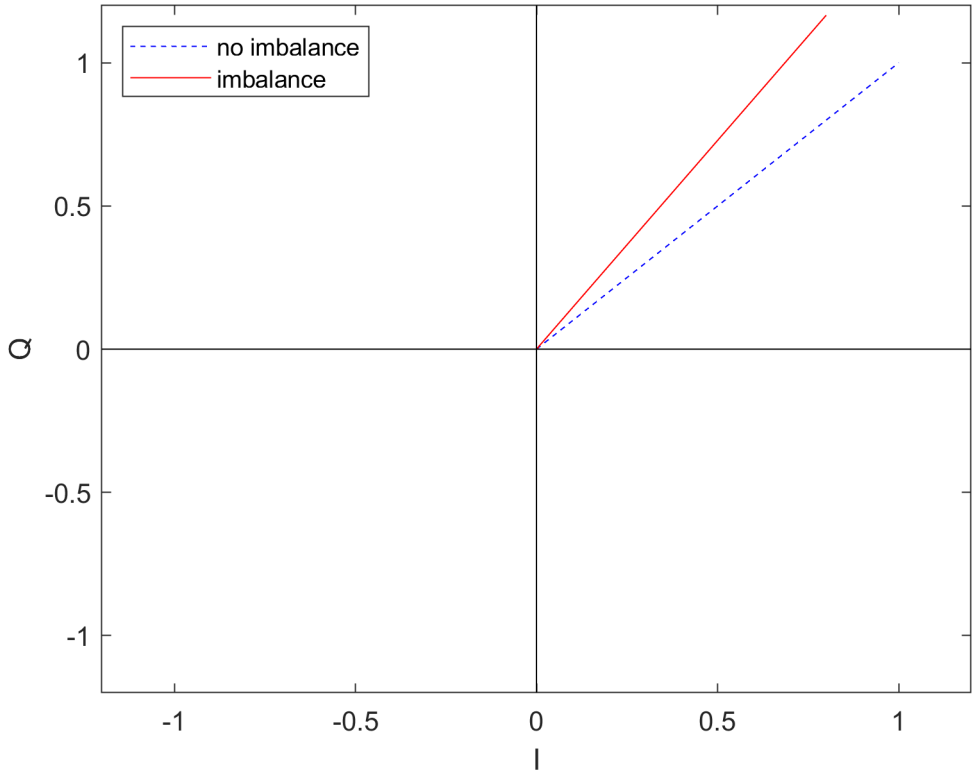

Figure 2.9: Vector representation of the IQ-imbalance

Figure 2.9 shows a vector representation of how the IQ-imbalance affects the in-phase and quadrature component. Where the angle $\alpha(\phi)$ between the no imbalance and imbalance depend on ϕ

To simulate the signal through the IQ-mixer, features is added to the signal considering IQ-imbalances. The IQ-imbalances originates from the non-idealities of the LO. This is simulated using equation (3.1) where the complex conjugate are considered in case of phase/amplitude shifts. This shift is a result of the I and Q in equation (2.5) and equation (2.6) being manipulated.

2.4 Amplifiers

As seen in Figure 2.10 there are two amplifiers present in the signal chain, one PA and one LNA. This is, as said before a simplified model where each amplifier block usually consist of a multi-stage amplifier. The output signal from the IQ-mixer is not strong enough to be transmitted. The PA boosts the signal to a level that can traverse to the receiver. This level is about 100dB higher than the received signal. Depending on the quality of the PA, more or less non-linearities will occur. The PA in a base-station introduces less non-linearities in comparison to a PA in a cell-phone. For this thesis a lower quality PA is used. The non-linearities is introduced in the simulation in different ways as shown in section 3.3

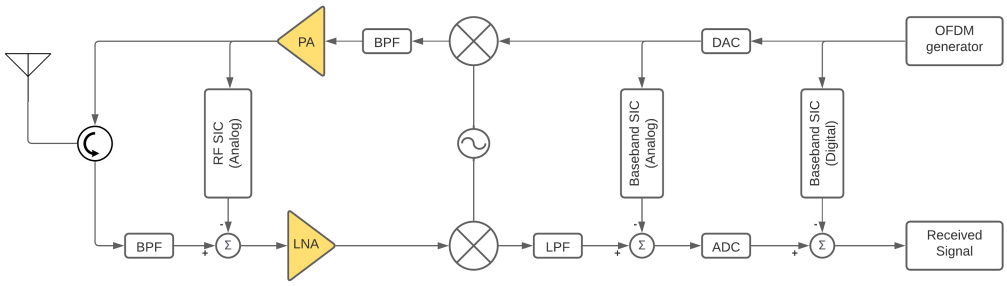

Figure 2.10: Block diagram of the simplified version of the transceiver, amplifiers highlighted

A good way of describing the characteristics of a power amplifier is with amplitude modulation to amplitude modulation (AM/AM) and amplitude modulation to phase modulation (AM/PM) characteristics. The AM/AM can be found by plotting the magnitude of the instantaneous gain as in equation (2.10) versus the instantaneous power of the input, which can be seen in figure 2.11.

$$|G(|x_{in}|)| = \frac{|x_{out}|^2}{|x_{in}|^2} = \frac{I_{out}^2 + Q_{out}^2}{I_{in}^2 + Q_{in}^2} \tag{2.10}$$

Similar to AM/AM, the AM/PM can be found by instead plotting the phase of the instantaneous gain as in equation (2.11) versus the input power, which can be seen in figure 2.12.

$$\angle G(|x_{in}|) = \angle x_{out} - \angle x_{in} \tag{2.11}$$

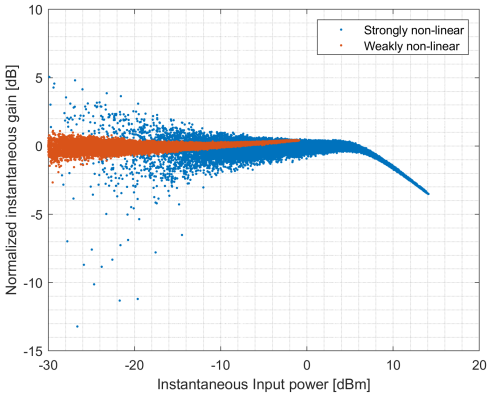

Figure 2.11: Normalized AM/AM characteristics of a power amplifier

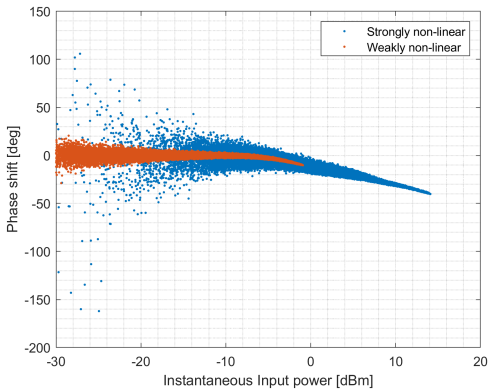

Figure 2.12: AM/PM characteristics of a power amplifier

A normalized AM/AM plot for a memory-less linear PA would be a horizontal line at 0dB, which means that the gain of the PA could be described as a constant. In figure 2.11 it can be seen that for a lower input power (orange) it is closed to being centered around 0dB which indicates that the output of the PA is weakly non-linear. The same indication of non-linearities can be seen from the AM/PM plot in figure 2.12. However, for higher input power (blue) it can be seen that it has about 4dB compression in the gain. The compression indicates that the output of the PA is non-linear.

In a memory-less system the output value at time t only depends on the input value at time t, for example a memory-less linear PA the output would be $y(t) = ax(t)$. However, a system with memory the output depends on the current input value at time t and at past values, for example a linear PA with memory the output could be $y(t) = a_1x(t) + a_2x(t-1)...$, which means the output also depends on past inputs. The dispersion in the AM/AM and AM/PM plots is a qualitative indication that there exist memory. Because for similar input values the corresponding output have a different value[16].

From figure 2.11 it can be seen that for higher input (blue) that in the non-linear region (input power above approximately 4dBm) there is less dispersion than in the linear region. This is an indication that there is more memory in the linear region than in non-linear.

The non-linear effect can also easily be seen from figure 2.13 which shows the spectrum of an OFDM signal with a bandwidth of 5MHz, both input and output. It can be seen that the output has frequency components outside of the bandwidth. Which means there are harmonics.

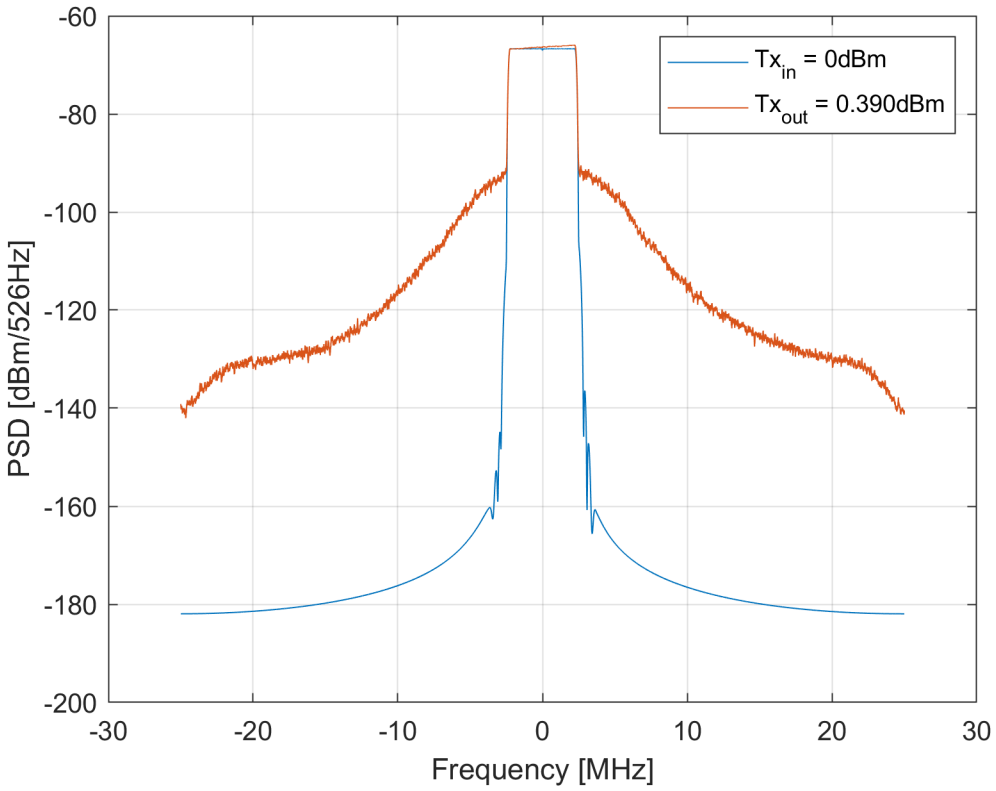

Figure 2.13: Differences between Tx in and Tx out

Frequency components that can not be distinguished from figure 2.13 are components that are due to a non-linear PA but are within the bandwidth. It can be shown with a two tone signal that non-linear effects occur within the band. Consider a two tone signal with frequencies f_1 and f_2 where $f_2 > f_1$, as in equation (2.12).

$$s_{in}(t) = A_1 cos(2\pi f_1 t) + A_2 cos(2\pi f_2 t) \tag{2.12}$$

If the two tone signal s_{in} is run through a third order non-linear system, the output would be

$$s_{out}(t) = s_{in}(t) + s_{in}^2(t) + s_{in}^3(t) \tag{2.13}$$

The frequency components that exists in s_{out} is shown in figure 2.14. Where the components with a frequency greater than f_2 is the components outside the band and the components less than f_2 are the components within the band, i.e. the dc, $f_2 - f_1$ and $f_2 - f_1$ components, for a third order system[16].

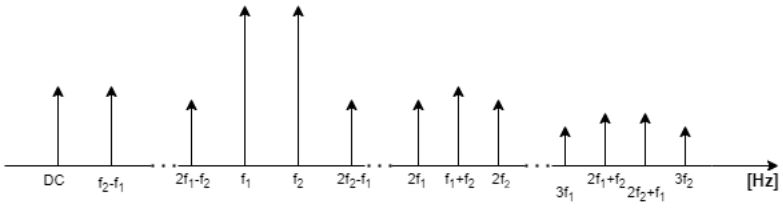

Figure 2.14: Output in frequency domain of a two tone input signal

The LNA boosts the power of the received signal above the noise floor. The noise figure therefore directly limits the sensitivity of the receiver [17]. The LNA is a high quality amplifier not adding any significant non-linearities that needs to be taken into account when simulating.

2.5 Bandpass and lowpass filters

Two bandpass filters are used. First a bandpass filter is used after the IQ-mixer on the transmitter side of the chain. For an IQ-mixer there is imbalances. The imbalances and imperfections creates harmonics, image and dc signal (from the even harmonics) that needs to be filtered out.

Another bandpass filter is used at the receiver side. With the isolation leakage combined with the received signal harmonics appears. The harmonics can be eliminated by using a bandpass filter. By using the bandpass filter directly after the circulator the LNA wont boost unwanted signals and the signals entering the IQ-mixer will only be of relevant frequencies.
Usually though, a BPF is used after the PA to remove harmonics and the BPF after the LNA is often there to reduce the wideband noise and increase the SNR.

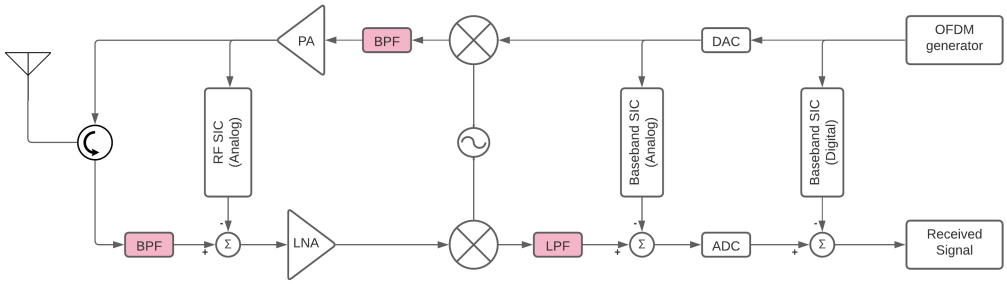

Figure 2.15: Block diagram of the simplified version of the transceiver, filters highlighted

The output of the IQ-mixer on the receiver side of the chain is similar to the bandpass filter after the IQ-mixer in the transmitter side of the chain. It is portrayed as a low pass filter even if it is basically is a bandpass filter. Basically is it a lowpass filter that also filters out the DC components.

2.6 RF SIC

The SI in the RF signal is cancelled in two different ways. There is the passive SIC and the active SIC, they are both built into the RF SIC block highlighted in figure 2.16

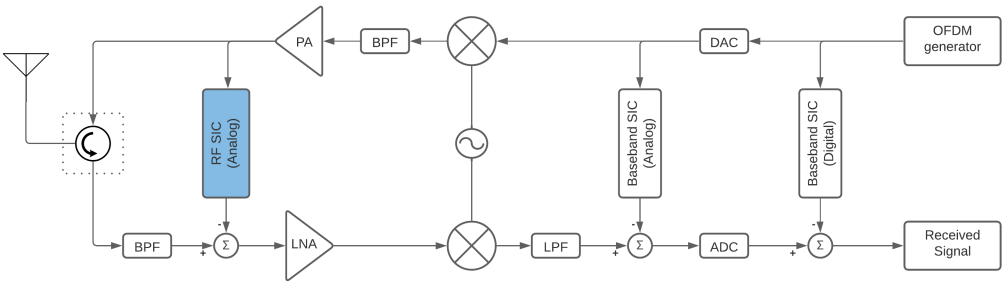

Figure 2.16: Block diagram of the simplified version of the transceiver, passive and active RF SIC highlighted

2.6.1 Passive RF SIC

The passive SIC uses different techniques to attenuate the RF signal. Dual-polarized antenna can be used for SI cancellation in RF. By changing the polarization of the antennas the signal can be attenuated [18]. The simplest way of attenuating the signal in analog RF is by physically isolate or move apart the transmitter from the receiver. If using a transceiver a circulator can be added. A circulator works as a one way street for the signal. Ideally letting the transmitted signal through to the antenna while blocking the transmitted signal towards the received signal chain side. This isolation is not however ideal and leakage of the transmitted signal is being combined with the received signal in the receiver side of the signal chain.

Studies have shown that dual polarized antennas can achieve an average of 90dB SI isolation at 300GhZ with a compact antenna size. [19]

Passive suppression is a big part in the analog RF cancellation. By isolating the transmitter from the receiver the line of sight radio signal between transmit antenna and receiver antenna is suppressed. This suppression can in certain environments be up to 70dB [20]. A reasonable level of suppression from the RF SIC is assumed to be around 20-40dB. The amount of supression depends on the bandwidth, the center frequency and the techniques used.
Another new RF SIC technique is the beamforming cancellation that is an evolving method [21] [22]. The idea is to reduce the output leakage reaching the receive array while transmitting. At the same time receiver-beamforming minimize the interference while receiving data. Beamforming cancellation uses antenna arrays that work together by transmitting and receiving with slight delays and different phase shifts which makes the signal the signal stronger in the given direction and weaker/undetectable in other directions. Researchers believe that the beamforming cancellation could potentially replace the analog cancellation, although they still envision that those two should work together [22]

2.6.2 Active RF SIC

The active RF SIC is necessary to attenuate the signal enough such that the LNA and/or the ADC is not saturated by SI. If either of those would be saturated the signal would be corrupt and unreadable. One Analog SIC method is the Analog Least Mean Square (ALMS)adaptive filter proposed in [23].

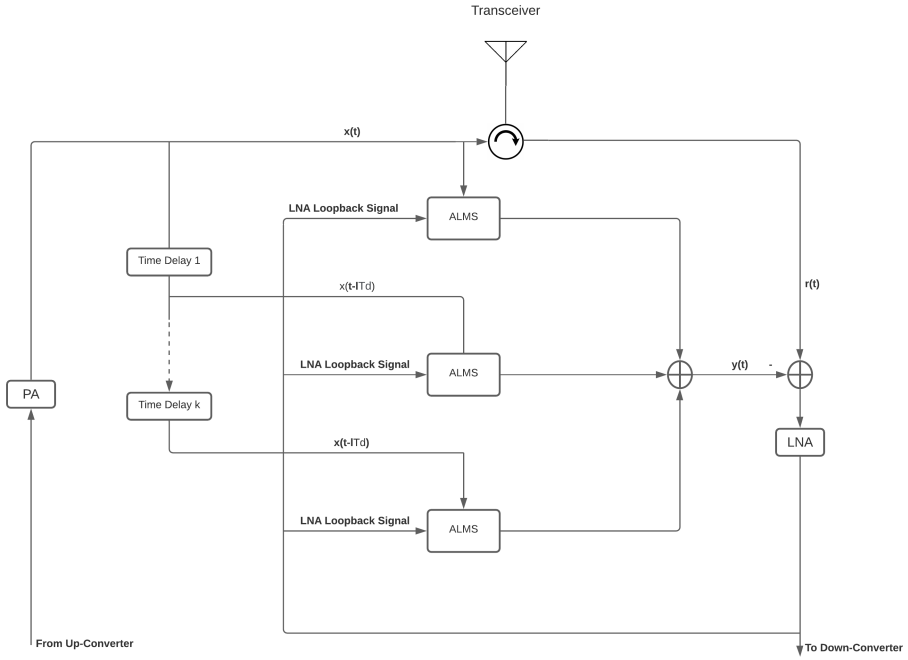

Figure 2.17: Block diagram of a ALMS loop with multi-tap adaptive filter

The ALMS multi-tap filter shown in figure 2.17 process the transmitted signal x(t) at different Time delays described as $x(t - lT_d)$ where T_D is the time delay and l is the number of time delays. The transmitted signal is together with the LNA loopback signal processed in the ALMS shown in figure 2.18.

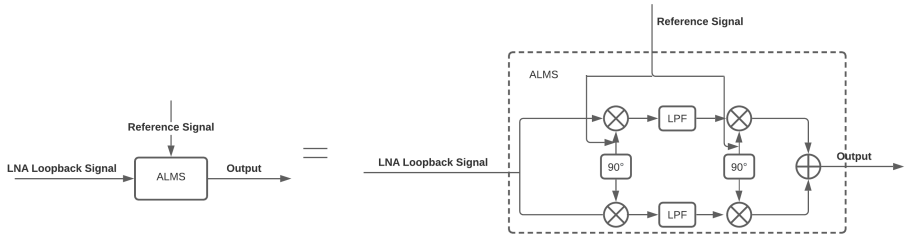

Figure 2.18: Block diagram of ALMS

The reference signal x(t) at different delay units T_D together with a LNA loopback signal enters the ALMS tap. The signals are I/Q demodulated and the product of the demodulated signals goes through a LPF. The ALMS works in a similar way as the digital processing, updating the weights of the complex coefficients, here without any digital signal processing. The updated weights modifies the delayed reference signal at the I/Q modulator. The weights together with their respective delayed reference signal combines to the cancellation that is subtracted from the received RF signal. This process is also described in figure 2.18

2.7 Analog SIC

Reaserchers have tried to add an additional analog SIC in the baseband. Analog baseband SIC is, much like the Analog RF SIC present to not saturate the ADC. An example of this is presented in [24]. This is a crucial step if the cancellation in the passband isn't high enough. There are several important factors that needs to be taken into account to assure that the ADC is not saturated.

- Power of the received signal
- Power of the SI

- Cancellation in the passband
- Number of bits in the ADC (see section:2.2)

$$SINR = P_r - (P_{SI} - P_{ac}) \tag{2.14}$$

The SINR after the LNA (assuming the LNA is not saturated) can be expressed as seen in equation (2.14) where P_r is the power of the received signal, P_{SI} is the power of the SI and P_{ac} is the total analog cancellation in the passband.
For the ADC the number of bits is directly related to the resolution of the signal. For example, an ADC with 12 bits can convert the signal to $2^{12} = 4096$ different integers, corresponding to amplitude intervals. The SINR in the baseband and the number of bits in the ADC is in this thesis assumed to be good enough to not saturate the ADC.

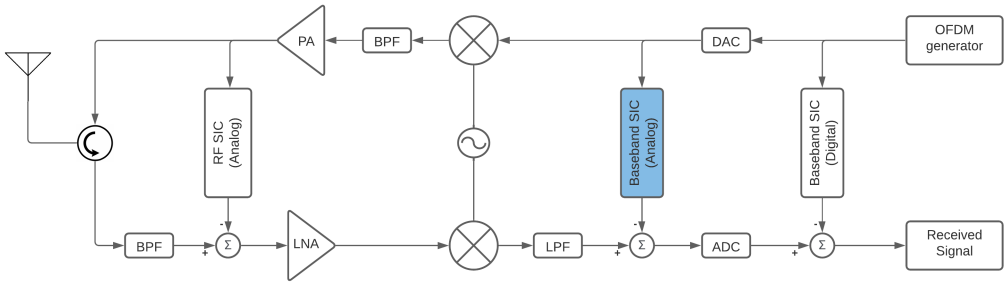

Figure 2.19: Block diagram of the simplified version of the transceiver, analog SIC block highlighted

In [25], a method is presented that solely relies on the RF SIC. This thesis follows the same procedure and skips the analog baseband SIC.

2.7.1 Digital SIC

The analog SIC is never perfect and the residuals has to be dealt with using digital SIC techniques. The digital cancellation is present to remove enough residuals for the signal to be understandable. The digital SIC is shown in figure 2.20.

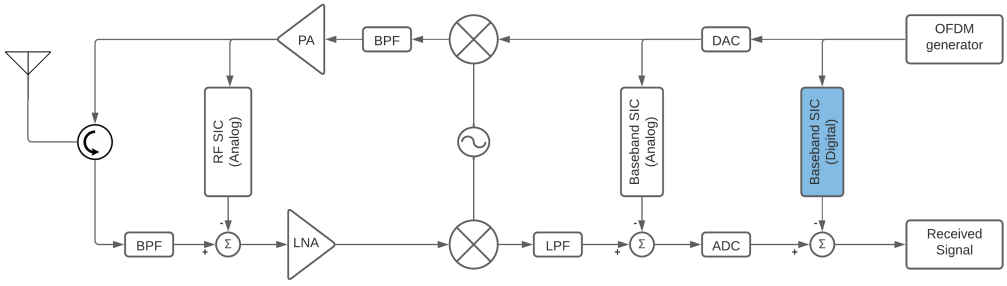

Figure 2.20: Block diagram of the simplified version of the transceiver, digital SIC block highlighted

To be able to cancel the signal in the digital domain the signal chain has to be modeled. This means that the transfer function of the system has to be estimated. This is done by estimating what manipulations has been done on the signal and creating features to represent each of the manipulations. After the features has been created the filter should be trained to evaluate weights for each of these features. The filter estimates a part of the whole signal to estimate weights and finally the weights together with their respective feature is subtracted from the signal to ideally only export the received signal to the demodulator without any residuals.
However, the reality is not as simple as the theory. The digital filter has to be quick enough to prevent any delays. This means the features has to be optimized and no unnecessary features should be added. The

environment constantly changes and therefore the filter should be adaptive to adjust for small changes as times goes by. This means the filter should be both quick and adaptive at the same time as the features should be minimized and still contain as much of the SI as possible.
If the analog cancellation is good enough such that neither the LNA nor the ADC is saturated the digital cancellation still has to cancel out the residuals quick enough and good enough for full duplex to work.

3 Modelling the signal chain

It is crucial to properly resemble the actual signal chain in the simulation as the weights solely depends on model training. Therefore modelling each part of the signal chain is critical. As the signal passes through each block in Figure 2.1, various manipulations of the signal are performed. Depending on the manipulations, different features are added to the filter. Weights for these features are then trained to resemble the actual system using different methods.
In this thesis the signal that is reconstructed is dependent on the following:

- The transmitted OFDM signal has a bandwidth of 5MHz and is provided by Syntronic.
- The received OFDM signal is generated using Matlab with a bandwidth of 50MHz separated into 512 subcarriers and later run through the experimental setup by Syntronic.
- The transmitted signal has an output power ranging from -9.82dBm to 3.73dBm
- The received signal has an output power ranging from -43.0dBm to -14.2dBm.
- The ADC,DAC and LNA are assumed to not be saturated in the data received from Syntronic
- The RF SIC attenuate the signal 65dB where 25dB is in a circulator and 40dB is pure attenuation representing the RF analog SIC.

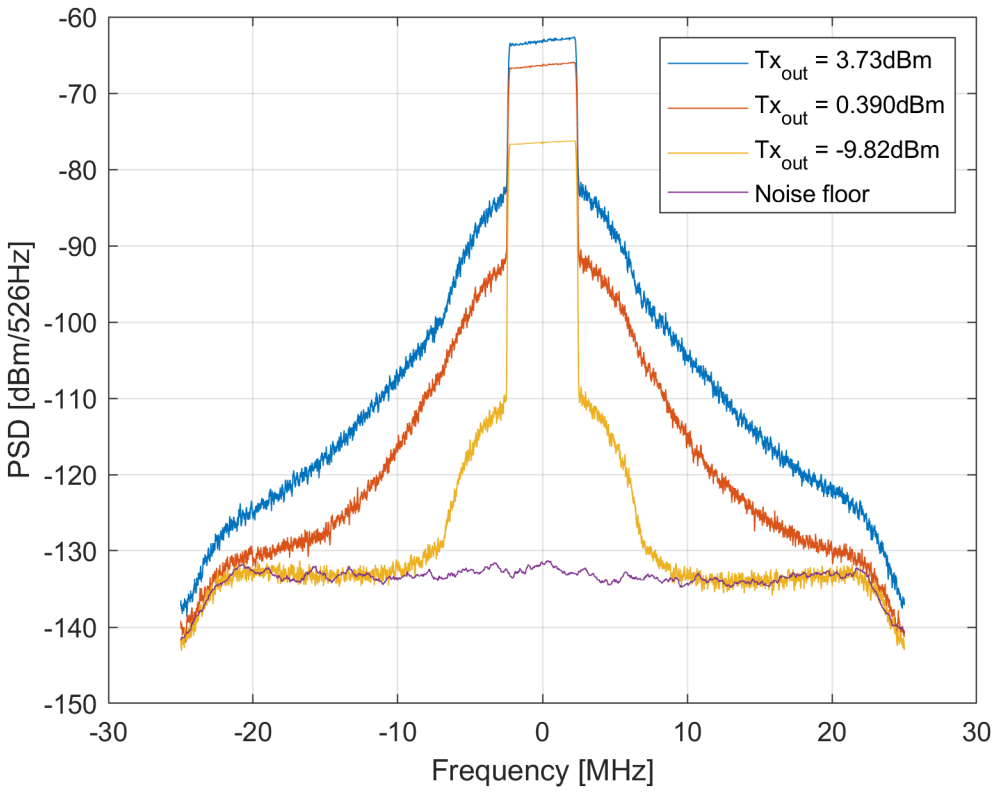

Figure 3.1: Power spectral density plot of received Tx with a bandwidth of 5MHz for 3 different input powers

In all the spectrum plots the y axis is displayed as dbm/526Hz, this is $\frac{dbm}{NsFs}$ where the number of samples (Ns) = 95040 and the sampling frequency (Fs) = 50e6.

For higher input power the SI is more non-linear which can clearly be seen in Figure 3.1. With an input power of 5dBm the output occupies a bandwidth of close to 50MHz. For an input power of -10dBm it can be seen that the SI is close to linear, it only occupies a bandwidth of about 10MHz.

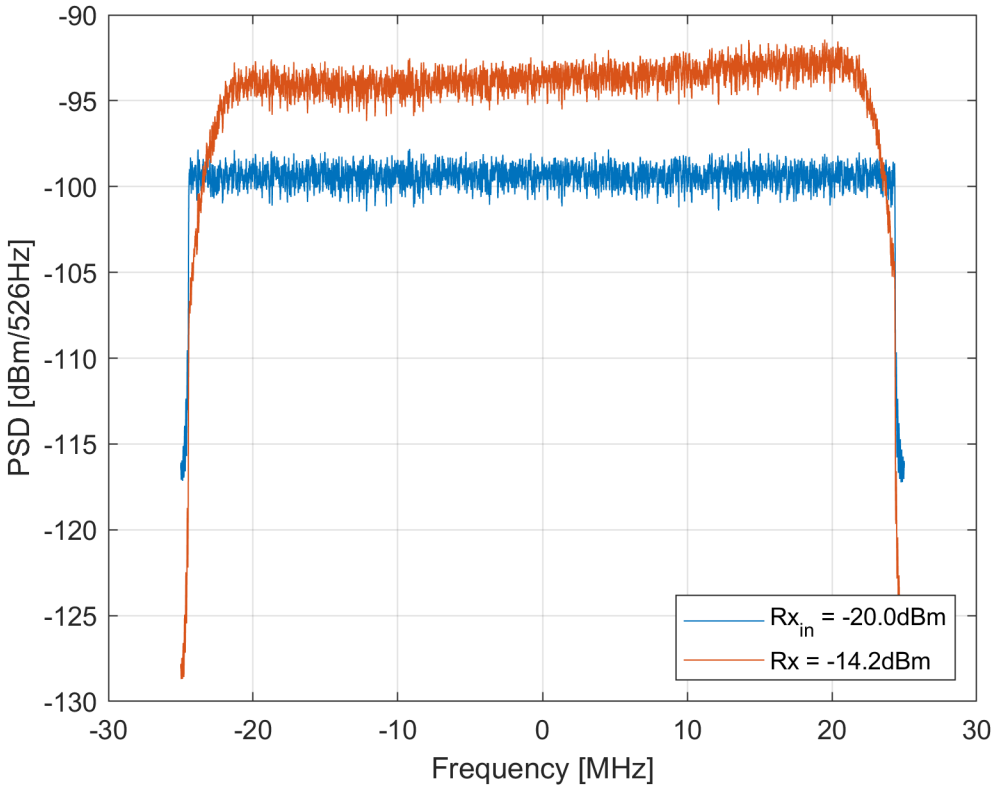

Figure 3.2: Power spectral density plot for rx input power = -20dBm and its corresponding rx output power

The PSD of Rx input power = -20dBm and it's corresponding output power -14.2dBm is shown in Figure 3.2. The output power is higher than the input power thanks to the LNA that amplifies the signal more than it is attenuated by the circulator in the measurement setup. The output power also has a bit narrower bandwidth because of the band-pass filter placed before the LNA to not amplify noise.

Rx [dBm]	SNR [dB]
-42.96	9.031
-38.69	13.90
-34.03	18.82
-29.17	23.95
-24.10	29.04
-19.14	34.05
-14.23	39.04

Table 3.1: Rx outputs with their respective SNR

In table 3.1 the Rx output power together with their respective SNR is displayed. The SNR vs Rx power is as seen linear meaning the measurements were done with a constant noise floor.

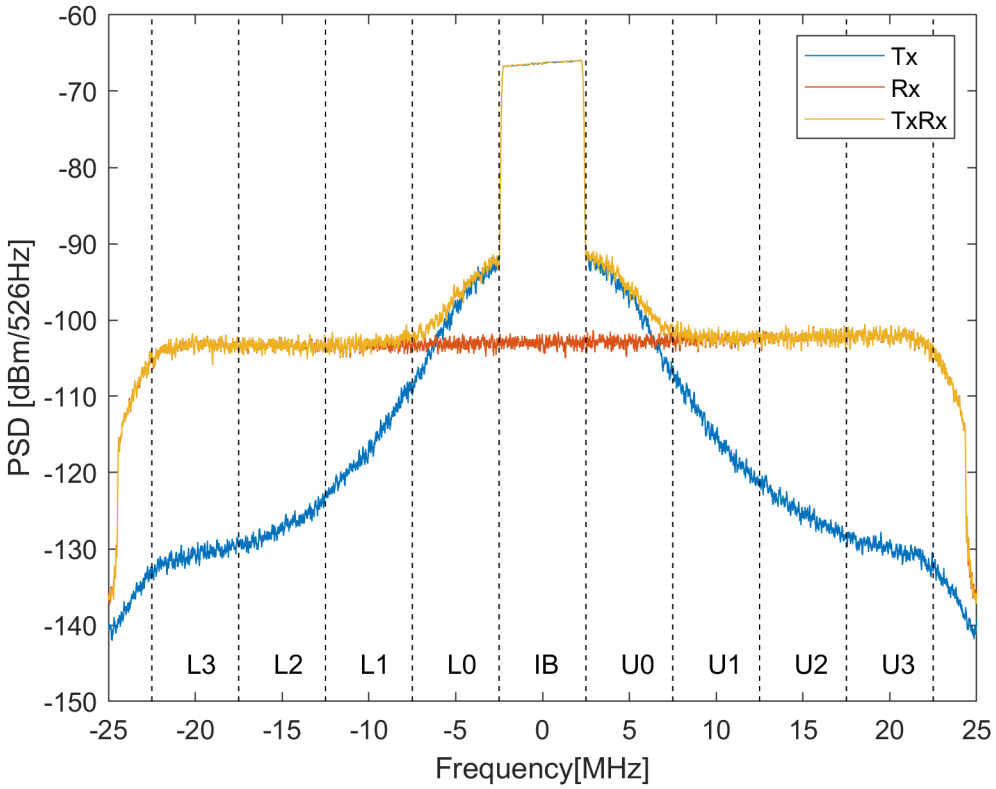

Figure 3.3: PSD for Rx, Tx and TxRx output power given Tx output power = 0.39dBm and Rx output power = -34dBm

In figure 3.3 the PSD is separated into In-band channel, adjacent channels and alternate channels named IB, [L0 U0] and [L1, L2, L3, U1, U2, U3] where IB stand for In band, L stand for lower and U stand for upper. TxRx is the combined signal from Tx and Rx in the receiving end of the signal chain. This is the signal that is processed in the cancellation. Tx, Rx and TxRx can be seen in figure 3.3. In this thesis the bandwidth for Rx is chosen to 50MHz and the bandwidth of Tx 5MHz. This makes it possible to separate the results for the in-band, adjacent and alternate channel cancellation. This is also done to check the non-linear cancellation which is the only present SI in the adjacent and alternate channels. Within the band both linearities and non-linearities are present. However, by doing a linear model the linear cancellation within the band can be estimated. It can also be seen that TxRx follows Tx within the bandwidth as a result of the difference between Tx and Rx being large. If the SI were low TxRx would follow Rx outside of the bandwidth outside of the bandwidth of Tx in comparison to what is presented in the figure where TxRx is slightly above Rx.

3.1 OFDM generator

The desired (received) signal is generated using the script generated by the OFDM waveform generator application in Matlab. The OFDM waveform generator can be seen in Figure 3.4. The data taken into consideration is the bandwidth, the sampling rate and number of samples of the transmitted signal. The bandwidth of the generated signal depends on the FFT length and the subcarrier spacing as $FFT_{length} * Subcarrier_{spacing} = Bandwidth$. The FFT length is the number of subcarriers plus the guard band. Where the guard band is subcarriers at the edge of the frequency spectrum without any data to prevent disturbances. The subcarrier spacing is the distance between each subcarrier in the frequency domain. For this thesis a pilot is manually created for reference as the initial OFDM symbol see section 2.1.2. More about how the pilot is used for demodulation is also described in section 3.6.

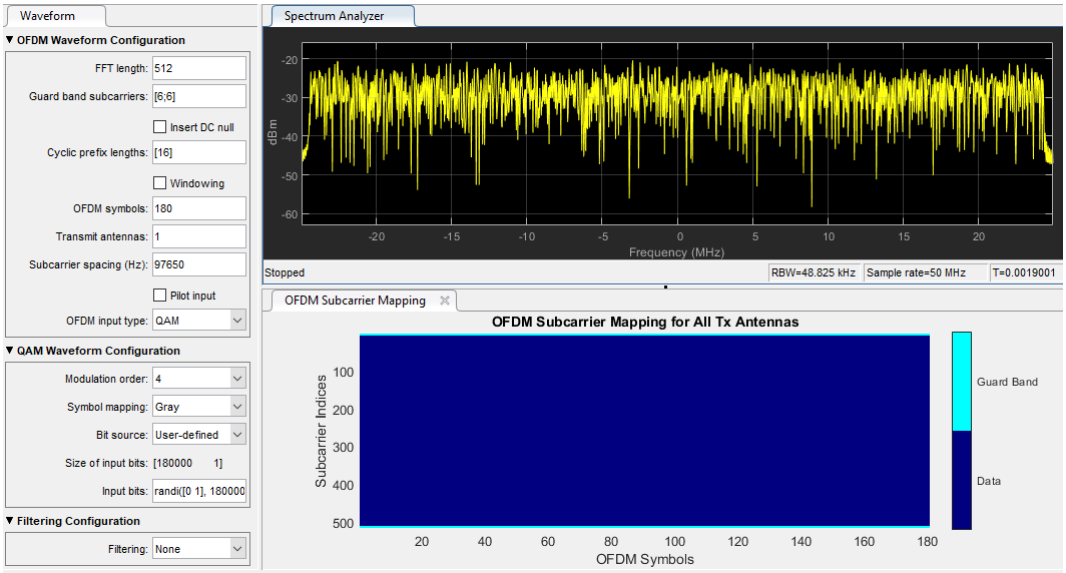

Figure 3.4: Graphical user interface for wireless waveform generator in Matlab

The received signal is created with a bandwidth of 50MHz compared to the transmitted signal which has a bandwidth of 5MHz. This is to compare the linear and the non-linear SIC. If the received signal had the same bandwidth as the transmitted signal the non-linearities that occurs outside of the bandwidth wouldn't matter and the non-linear cancellation for frequencies outside of the bandwidth could simply be filtered out using a bandpass-filter and the modeling of the non-linearities of the signal would be hard the estimate.
A bitstream is randomly generated as graycoded input. The bitstream is saved as reference of the actual desired signal for later comparison.

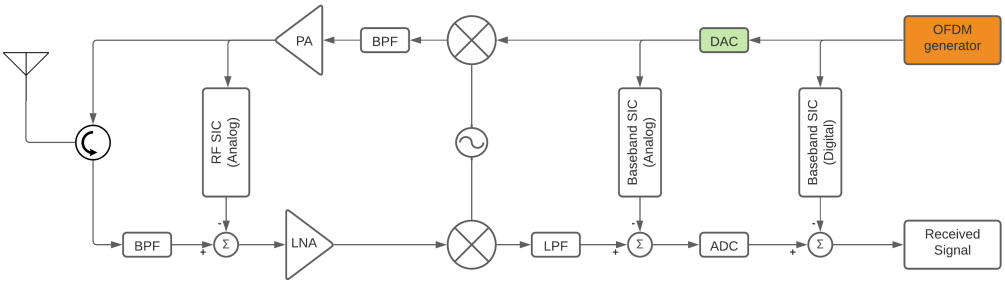

Figure 3.5: Block diagram highlighting the OFDM generator together with the DAC

3.2 IQ-mixer

In the IQ-mixer the in phase component and quadrature component are up-converted to RF frequency via two local oscillators (LO), where the quadrature components LO is ideally 90° out of phase. However, in the real case there will be some imbalance. This can be modelled with equation (3.1), which models both the mixer imbalance and the gain imbalance from the LO. These features will compensate for the phase offset and the gain offset from the IQ-mixer[26].

$$\hat{x}_{IQ}[n] = g_1[n]x[n] + g_2[n]x[n]^*, \tag{3.1}$$

where $x[n] = I[n] + jQ[n]$, g_1 is the response for the direct component and g_2 is the response for the mirrored image complex conjugate of the direct component. Here * denotes complex conjugate.

It can be shown that equation (3.1) is a good way of modelling the imbalance of the IQ-mixer since $x_{IQ}[n] = \hat{I}[n] + i\hat{Q}[n]$ (from equation (2.9)) can be represented by equation (3.1) because there is a g_1, g_2 for a specific ϕ such that $\hat{x}_{IQ} = x_{IQ}$.

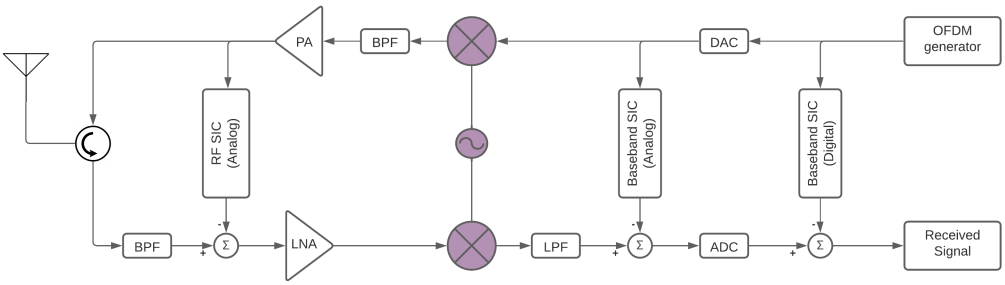

Figure 3.6: Block diagram of the signal chain, IQ-mixer highlighted

3.3 Power Amplifier

The largest distortion of the signal is happening in the PA. Several ways of modelling the PA have been studied in previous researches [27] [28] to model the features that are being added to the signal. The different features that are added to the model is either polynomial features, cross term features or memory features. Three ways of modeling the PA are presented below.

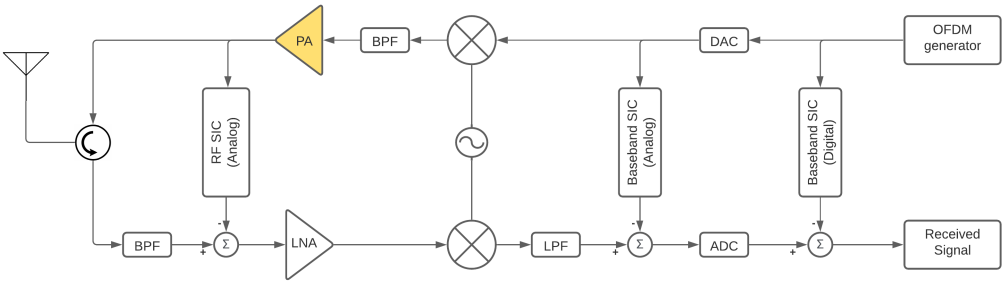

Figure 3.7: The amplifiers of the signal chain

3.3.1 Memory polynomial model

One way to model the PA is with a memory polynomial based model, which can be described as a linear regression model

$$y(n) = \boldsymbol{\psi}(n)\boldsymbol{\theta}, \tag{3.2}$$

where $y(n)$ is the output of the model, $\boldsymbol{\psi}(n)$ is a feature row vector built with baseband input signal samples and $\boldsymbol{\theta}$ is a column vector containing the model coefficients.

The feature vector $\boldsymbol{\psi}(n)$ can contain non-linear functions of the signal but the model is still linear with respect to its coefficients. Since all memory polynomial models are linear to its coefficients this makes it possible to use linear identification techniques.

3.3.2 Volterra

Volterra series is similar to the Taylor-expansion. Volterra series however uses the memory and the output of the nonlinear system depends on the input to the system at all other times. This allows Volterra to capture the "memory" effect. In our system that is the memory manipulated by the Power Amplifier (PA).

$$x_{PA} = \sum_{k=0}^{N} h_k x_k + \sum_{k_1=0}^{N}\sum_{k_2=0}^{N} h_{k_1,k_2} x_{k_1} x_{k_2} + \sum_{k_1=0}^{N} \dots \sum_{k_p=0}^{N} h_{k_1,\dots,k_p} x_{k_1} \dots x_{k_p} \tag{3.3}$$

The full Volterra series expansion is showed in equation (3.3). Here, x_k is the input at time x(n-k), h_k is the weight for the given term and N is the number of memory that will be considered.

This also includes the products with different time-shift, called cross terms to avoid non-uniqueness in the model, equal cross terms are combined with a shared weight as explained in equation (3.4)

$$\begin{aligned} h(k_1,k_2)x(n-k_1)x(n-k_2)+h(k_2,k_1)x(n-k_2)x(n-k_1) = \\ = h'(k_1,k_2)x(n-k_1)x(n-k_2) \end{aligned} \tag{3.4}$$

3.3.3 Memory Polynomial (MP)

One way to model a power amplifier is with a MP model as seen in equation (3.5). This is a simplified version of the Volterra series, where the cross terms are excluded which results in a less accurate model compared to the Volterra. However, since the cross terms are excluded both the order P and the number of memory taps M can be larger and still have a much lower computational complexity compared to Volterra. This is a trade-off between computational complexity and model accuracy.

$$x_{PA}(n) = \sum_{p=1}^{P}\sum_{m=0}^{M} h_{PA}(p,m)x(n-m)|x(n-m)|^{p-1} \tag{3.5}$$

Where p=*odd* is the order of the non-linearities, M is the memory and $h_{PA}(p,m)$ is the impulse response at the p-*th* order with memory m

Equation (3.5) can be described with (3.2) as

$$x_{PA}(n) = \boldsymbol{\psi}_{PH}(n)\boldsymbol{\theta} \tag{3.6}$$

where

$$\boldsymbol{\psi}_{PH}(n) = \begin{bmatrix} x(n) \\ x(n-1) \\ \vdots \\ x(n-M) \\ x(n)|x(n)|^1 \\ \vdots \\ x(n-M)|x(n-M)|^{P-1} \end{bmatrix}^T \tag{3.7}$$

and

$$\boldsymbol{\theta} = \begin{bmatrix} h_{PA}(1,0) \\ \vdots \\ h_{PA}(P,M) \end{bmatrix} \tag{3.8}$$

3.3.4 Generalized Memory Polynomial

The Generalized Memory Polynomial (GMP) is a model that is in between of the MP and the Volterra model. The Volterra model contains all the features possible and Hammerstein contains the exponential terms. For the GMP a given set of features are used. The number of features can be modified and trimmed as hyper-parameters in the simulation to find a good balance between result and computational complexity.

$$\begin{aligned} x_{pa}(n) = &\sum_{p=1}^{P_a}\sum_{m=0}^{M_a} h_{a,pm}x(n-m)|x(n-m)|^{p-1} \\ &+\sum_{p=2}^{P_b}\sum_{m=0}^{M_b}\sum_{k=1}^{k_b} h_{b,pmk}x(n-m)|x(n-m-k)|^{p-1} \\ &+\sum_{p=2}^{P_c}\sum_{m=0}^{M_c}\sum_{k=1}^{k_c} h_{c,pmk}x(n-m)|x(n-m+k)|^{p-1} \end{aligned} \tag{3.9}$$

The first term in equation (3.9) is exactly like the MP, the second and third terms are the leading and lagging cross-terms.

Usually not all coefficients are needed. For example, the odd order nonlinearities usually dominates and therefore the even order non-linearities can be excluded. Or that the number of memory taps varies with different orders. To be able to model the PA more accurate and/or reduce the computational complexity equation (3.9) can be rewritten with index arrays, as in equation (3.10)[29].

$$\begin{aligned} x_{pa}(n) = &\sum_{p\in p_a}\sum_{m\in m_a} h_{a,pm}x(n-m)|x(n-m)|^{p-1} \\ +&\sum_{p\in p_b}\sum_{m\in m_b}\sum_{k\in K_b} h_{b,pmk}x(n-m)|x(n-m-k)|^{p-1} \\ +&\sum_{p\in p_c}\sum_{m\in m_c}\sum_{k\in K_c} h_{c,pmk}x(n-m)|x(n-m+k)|^{p-1} \end{aligned} \tag{3.10}$$

3.4 RF SIC

In this thesis, no antenna is used but instead a decoupler to represent the antenna. This removes the option of using antenna separation or dual polarization methods. Instead a circulator is added as isolation between the transmitted signal and the received signal. As mentioned in section 2.6.1 the circulator works as an isolator between the transmitted and the received signal.

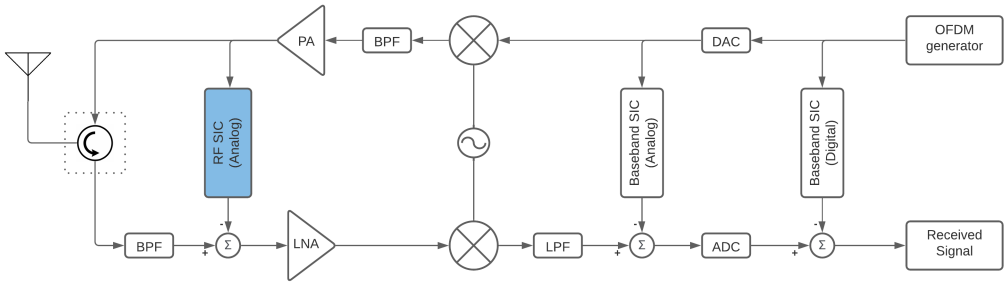

Figure 3.8: Block diagram of the signal chain, RF SIC and circulated highlighted

This is modelled using data provided by Syntronic SRD. The data was measured on a circulator. The data was received in two parts, the gain and phase offset from port 1 to port 2 as well as from port 2 to port 3. A combined bode plot for the data can be seen in Figure 3.9.

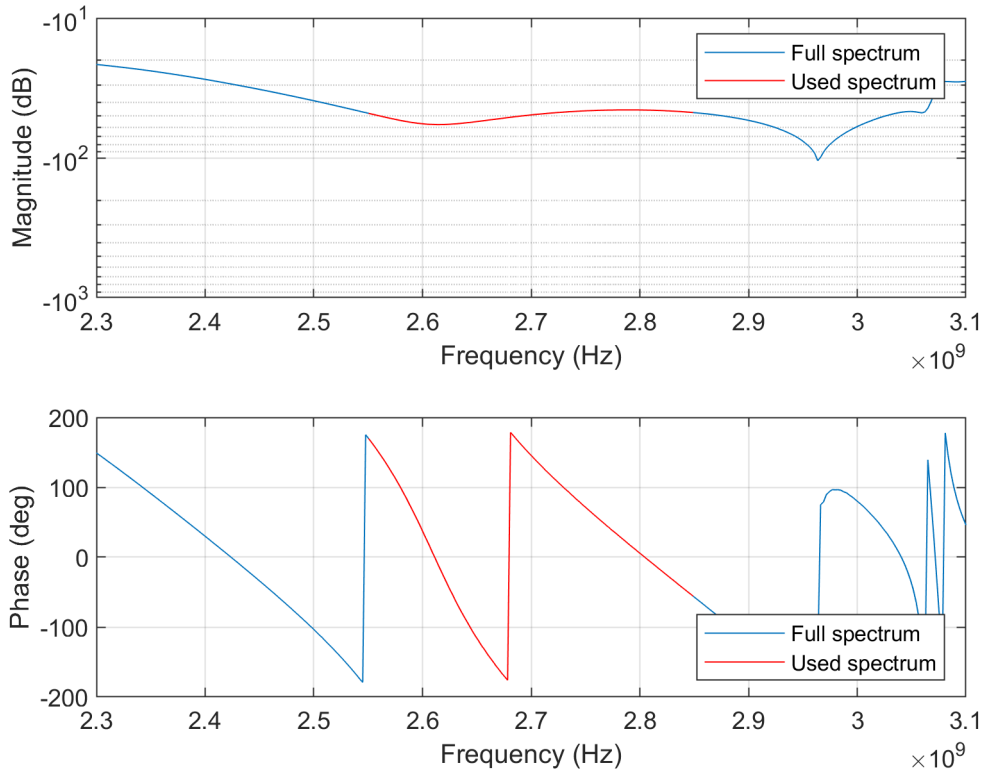

Figure 3.9: Bode plot of the frequency response of the SI-signal in the circulator

As the signal contains a higher resolution than the circulator measurements the signal is interpolated to fit the attenuation and the phase shift of each frequency. The transmitted signal is Fourier transformed to the frequency domain. Then it is attenuated using the interpolated gain of the frequency response as well as phase shifted using the interpolated phase shift of the frequency response. Finally the transmitted signal is being inverse Fourier transformed back into the time domain and the attenuated, phase shifted SI-signal is later added to the desired signal. This can further be explained as $SI_a(jw) = H_c(jw) * SI(jw)$ where $H(jw)$ is the transfer function of the circulator, $SI(jw)$ is the Fourier transformed transmitted signal $SI(t)$ and $SI_a(jw)$ is the attenuated and phase shifted signal that leaks through to the receiver side. $H_c(jw)$ is estimated as $\hat{H}_c(jw)$ through interpolation of the measured data.

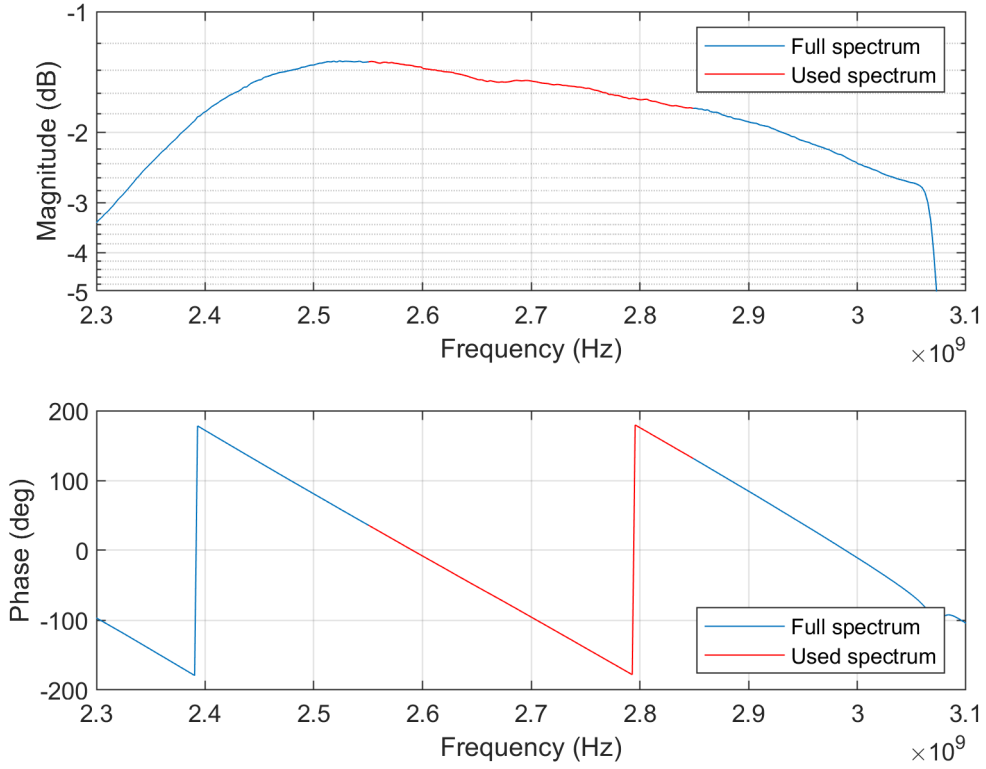

Figure 3.10: Bode plot of the frequency response of the desired signal in the circulator

The circulator also results in attenuation of the desired signal in the same way as the SI-signal. Since the signal is linear it means there is a constant group delay. The bode plot of the frequency response for the desired signal is shown in Figure 3.10. In the bode plots it can be seen that the circulator used in this thesis is working best around 2.6GHz. Figure 3.9 shows high attenuation for the SI whereas Figure 3.10 shows a low attenuation for the desired signal. Also the linear phase shift of the circulator makes it easier to interpolate the phase correction.

3.5 Low-pass filter

The non-linearities that occur also introduce components at higher frequencies. When frequencies are multiplied together in the GMP their frequencies add together. This means that aliasing will occur if the bandwidth of the feature is larger than the sampling frequency.

$$feature = x(t) * |x(t)|^p \tag{3.11}$$

An example of this is shown in equation (3.11). If $x(t)$ has a bandwidth of B and the term $|x(t)|^p$ has a bandwidth of $B * p \leq F_s$ then the feature in equation (3.11) will have a bandwidth of $B_{feat} = B + B * p$ and if the feature has a higher bandwidth than the sampling frequency F_s (i.e. $F_s < B_{feat}$) there will occur aliasing. To prevent this a digital low-pass filter as used as:

$$feature = x(t) * LP(|x(t)|^p) \tag{3.12}$$

where the low-pass filter LP is chosen such that $F_s \geq B_{feat} = B + LP(B * p)$.
These components are filtered using the built in low-pass filter in Matlab [30]. Where the filter is specified as an infinite impulse response filter which is preferred for a low-pass filter [31]. The low-pass filter is designed using the Type-2 Chebyshev Filter and in this thesis part of the digital SIC.

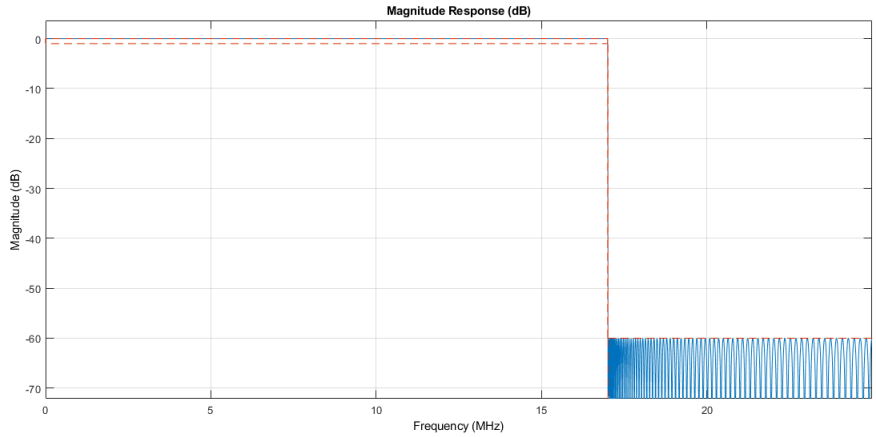

Figure 3.11: Frequency response of the filter

Figure 3.11 shows the frequency response of the low-pass filter using the built in tool "fvtool" for designed filters in Matlab. Chebyshev type-2 filters achieve a faster roll-off by allowing ripple in the stopband. The stopband ripple increases with increasing rolloff steepness and as seen in figure 3.11 is visible in the stopband [32]. An alternativ would be the Chebyshev type-1 filter that, compared to chebyshev type-2 has equiripple in the passband instead of in the stopband. [33].

3.6 Pilot

One of the big obstacles in wireless communication is to identify when the signal arrives. As described in section 2.1.2 a reference signal, also called a pilot is used. In this thesis an OFDM-symbol pilot is used. This means a complete OFDM-symbol is used as a reference signal. The pilot is made periodic by setting every other sample to zero. The rest of the signal is set to random using a known seed making it possible to reconstruct the exact same pilot every time. Ten OFDM symbols with the initial pilot can be seen in figure 3.12. It can be seen that the pilot is a periodic signal with periods $N/2$, where N is the number of samples in one OFDM symbol. One of the criteria for the pilot to make it realistic is to have a Peak to Average Power Ratio (PAPR) of at least below 12dB. Where the value 12dB was requested from Syntronic SRD who provided the data, however the lower the better. The PAPR is dependent on the instruments that is used in the measurements. This is to make the PA able to amplify smaller powers as well.

$$PAPR = Peak_{pwr} - Mean_{pwr} \tag{3.13}$$

Where $Peak_{pwr} = \frac{10log10(max(abs(data))^2)}{50}$ is the highest power at any datapoint measured in dB. $Mean_{pwr} = \frac{10log10(mean(abs(data))^2)}{50}$ is the average power measured in dB and the PAPR is in dB. Where 50 is the size of the resistor (50 ohm)

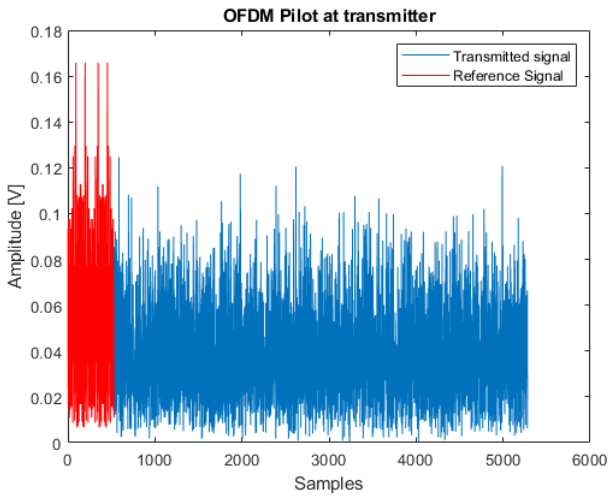

Figure 3.12: 10 OFDM symbols with a Pilot as the initial OFDM symbol at the transmitter end

To find out when the signal start, the pilot is identified using the periodicity described earlier. The received signal contains a lot of self-interference.

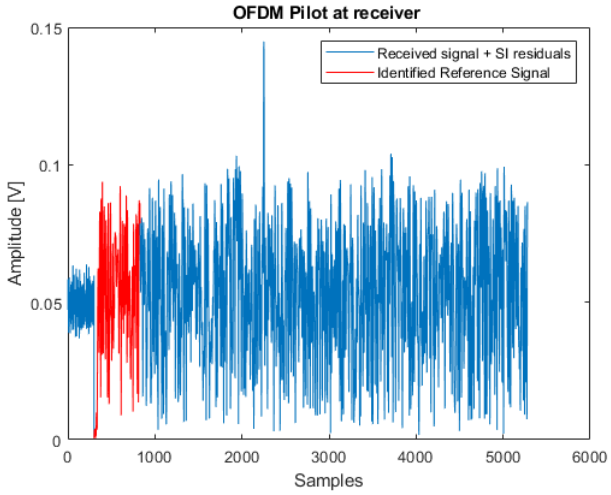

Figure 3.13: 10 OFDM symbols with a Pilot as the initial OFDM symbol at the receiver end

An example of this is displayed in Figure 3.13. Here the signal contains both the received signal and the residuals of the SI after the cancellation. The signal is identified by looking for where the signal contains the most auto-correlation. A sample with the highest auto-correlation is found within the cyclic-prefix from the start of the pilot. As the received signal reaches the end of the signal chain the signal is being downconverted to the generated rate. The signal is then demodulated to QAM symbols. The symbols are converted to binary numbers that are compared with the generated input bitstream to find out the BER of the system.

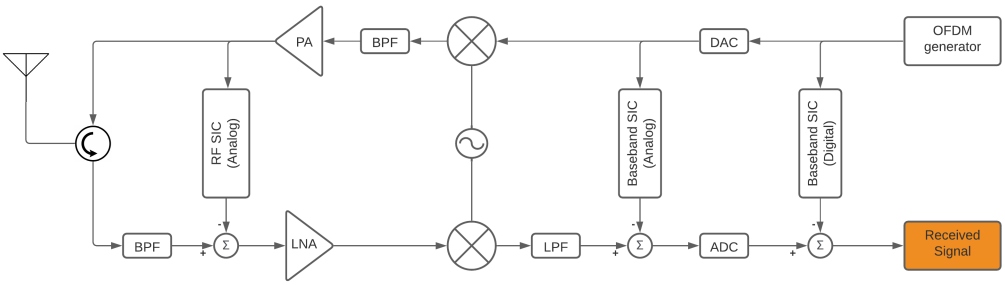

Figure 3.14: Block diagram of the signal chain, Received signal highlighted

The received signal can be seen at the end of the signal chain in figure 3.14

3.7 Evaluation measures

3.7.1 MSE

Mean squared error (MSE) is a measure of how close the estimated values are to the actual values. MSE is non-negative and a value closer to zero is better.

$$MSE = \frac{1}{n}\sum_{i=1}^{n}(Y_i - \hat{Y}_i)^2 \tag{3.14}$$

MSE can be used to compare the goodness of models, where $\hat{Y}_i$ is the output of a model and Y_i is the actual output. This mean $\hat{Y}_i$ is an estimate of Y_i.

3.7.2 BER

BER is the percentage of bits that are wrong after demodulation where BER = 1 mean 100% error and BER = 0 mean all bits are correct. If the signal only consists of noise the BER is 0.5 = 50%.

$$BER = \frac{e}{N} \tag{3.15}$$

Where e is the number of incorrect bits and N is the total number of bits.

3.7.3 SNR and SINR

SNR is a measure that compares the ratio between the power of the desired signal and the noise power. A SNR greater than 0dB means that the power of the desired signal is greater than the noise power.

$$SNR_{dB} = 10log_{10}\left(\frac{P_r}{P_n}\right) \tag{3.16}$$

Where P_r is the power of the received signal and P_n is the noise power within the bandwidth.

Signal to interference plus noise ration(SINR) is a measure like SNR but instead it is the ratio between the power of the desired signal and noise power plus interference power.

$$SINR_{dB} = 10log_{10}\left(\frac{P_r}{P_I + P_n}\right) \tag{3.17}$$

Where P_I is the power of the interference.

3.7.4 Path loss

Wireless radio channels is not only susceptible noise and interference but also channel impediments, such as path loss and shadowing. The path loss is caused by the power dissipation from the transmitter and also effects of the propagation channel. Shadowing is caused by obstacles between the transmitter and the receiver, which the attenuates the signal power through absorption, reflection, scattering and diffraction. Calculating the propagation channel is complex and often close to impossible, therefore simplified approximation models have been developed. A simple and commonly used model is the simplified path loss model, which is a path loss model as a function of distance.

$$P_r = P_t K \left(\frac{d_0}{d}\right)^{\gamma} \tag{3.18}$$

Where K is a constant that depends on the average channel attenuation and antenna characteristics, d_0 is a reference distance for the antenna far field. d_0 is typically assumed to be in the range 1-10m indoor and 10-100m outdoor. P_t and P_r is the power of the signal at the transmitter and the receiver respectively and d is the distance between them. γ is the path loss exponent that depends on the environment, which typically is in the range of $1.6-6.5$. Path loss exponents for some environments are shown in table 3.2 [9]

Table 3.2: Typical path loss exponents for some environments

Environment	γ range
Urban macrocells	3.7-6.5
Urban microcells	2.7-3.5
Office building (one floor)	1.6-3.5
Office building (multiple floors)	2-6
Home	3

The free space path loss gain P_L can be used as an approximation for the constant K

$$P_L = K = \left(\frac{\sqrt{G_l}\lambda}{4\pi d_0}\right)^2 \tag{3.19}$$

Where $\lambda = \frac{c}{f_c}$ is the wave length of the carrier frequency and $\sqrt{G_l}$ depends characteristics of the transmit and receive antenna ($\sqrt{G_l} = 1$ for omnidirectional antennas)[9].

By rearranging equation (3.18) it can be used as a rough measure of transmission distance.

$$d = d_0 \left(\frac{P_t K}{P_r}\right)^{1/\gamma} \tag{3.20}$$

4 Methods

With the feature matrix $\boldsymbol{\psi}(t)$ the linear coefficients $\boldsymbol{\theta}(t)$ needs to be estimated. There are numerous methods that can be used to estimate the coefficients $\hat{\boldsymbol{\theta}}(t)$. In this thesis three different methods are tested and evaluated. NLMS, OLS and RLS. The methods are tested thoroughly. The hyper-parameters are tuned for both the methods as well as the features of the PA, described in Section 3.3. RLS and LMS are both adaptive filters compared to OLS. This means they could tune the filter in real time. This is necessary if the environment is changing. With wireless communication there is a lot of changes in the environment because of the transmitter and/or receiver is moving.

4.1 Normalized Least Mean Square

The Normalized Least Mean Square (NLMS) algorithm is an adaptive filter based on the method of steepest descent. It is used to reconstruct the desired filter by finding the filter coefficients using the error signal. The NLMS of the error signal is the difference between the reconstructed signal and the actual signal. As an adaptive filter it uses the error at the current time and updates the weights over time. Therefore NLMS can take batches of data at a time to tune the filter, adapting to environmental changes and potentially achieve better result compared to a non-adaptive filter, especially if the surroundings change.
The idea of the NLMS algorithm is to update the weights based on the error between the estimated and the actual signal using NLMS. A feature vector ψ is modelled as described in section 3.

$$\hat{\boldsymbol{\theta}}(n+1) = \hat{\boldsymbol{\theta}}(n) + \mu(n)e^*(n)\boldsymbol{\psi}^T(n) \tag{4.1}$$

The weights are updated using equation (4.1). Here, $\hat{\boldsymbol{\theta}}$ is the estimated weights (or the initialized weights for n=0). μ is adaptive step length, e is the error and $\boldsymbol{\psi}$ is the feature vector.

There is generally two ways to initialize the weight vector. The first way is if you have information regarding how the features should be weighted and by using the prior to initialize the weights. The other way, as used in this thesis is when there is no prior information regarding the weights. The weights are then initialized as a zero vector.

To assure convergence of the weights, the step size μ must be in the range

$$0 < \mu < \frac{1}{Tr(R_{\psi\psi})} \tag{4.2}$$

Where $tr(R_{\psi\psi}) = ||\boldsymbol{\psi}||_2^2$.

$$\mu = \frac{\boldsymbol{\beta}}{||\boldsymbol{\psi}||_2^2 + \epsilon} \tag{4.3}$$

The step size is updated following equation (4.3). Where ϵ is small to assure stability and β is in the range $0 < \beta \leq 1$. However, it is wise to have different step size μ for different features[34]. Three different step sizes were chosen, μ_{DC} for the DC feature, μ_{lin} for the linear features and μ_{nl} for the non-linear features. The vector representation of this can be seen in equation (4.4).

$$\boldsymbol{\mu}(n) = \begin{bmatrix} \mu_{DC}(n) \\ \mu_{lin}(n) \\ \vdots \\ \mu_{lin}(n) \\ \mu_{nl}(n) \\ \vdots \\ \mu_{nl}(n) \end{bmatrix} \tag{4.4}$$

With different step size for different features equation (4.1) instead is

$$\hat{\boldsymbol{\theta}}(n+1) = \hat{\boldsymbol{\theta}}(n) + \boldsymbol{I}\boldsymbol{\mu}(n)e^*(n)\boldsymbol{\psi}^T(n), \tag{4.5}$$

where $\boldsymbol{I}$ is the identity matrix.

$e^*(n)$ is the complex conjugate of the error from equation (4.6)

$$e(n) = y(n) - \boldsymbol{\psi}(n)\hat{\boldsymbol{\theta}}(n), \tag{4.6}$$

which is the difference between the measured SI $y(n)$ and the modeled SI $\boldsymbol{\psi}(n)\hat{\boldsymbol{\theta}}(n)$.

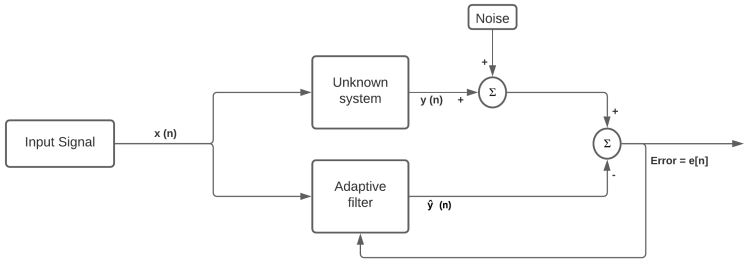

Figure 4.1: Block diagram of the LMS filter

This is also presented in a block diagram in Figure 4.1. Where the input signal $\boldsymbol{x}(n)$ passes through the adaptive filter. The feedback from the error signal is used to update the filter weights which are multiplied with the feature vector. The estimated output signal $\hat{y}$ is compared with the actual output signal y and the error is once again fed back to the adaptive filter to improve the weights.

4.2 Ordinary Least Square

The Ordinary Least Square (OLS) method estimates weights based on the squared error. The least square error (LSE) is found by minimizing equation: (4.7).

$$J(\theta) = \sum_{n=0}^{N-1} (y[n] - s[n])^2 = \boldsymbol{(y - \psi\theta)^H (y - \psi\theta)} \tag{4.7}$$

where $y[n] - s[n] = e[n]$ is the error at time n, $\boldsymbol{y}$ is the vectorization of the measured data. $\boldsymbol{\psi}$ is the features vector and $\boldsymbol{\theta}$ is the weights.

This is done by taking the gradient to $\boldsymbol{(y - \psi\theta)^H (y - \psi\theta)}$ [35]. The gradient can be seen in equation (4.8).

$$\frac{\partial J(\boldsymbol{\theta})}{\partial \boldsymbol{\theta}} = -2\boldsymbol{\psi}^H\boldsymbol{y} + 2\boldsymbol{\psi}^H\boldsymbol{\psi\theta} \tag{4.8}$$

Setting the gradient to zero yields the LSE. Which is the equation used in the simulation.

$$\hat{\boldsymbol{\theta}} = (\boldsymbol{\psi}^H\boldsymbol{\psi})^{-1}\boldsymbol{\psi}^H\boldsymbol{y} \tag{4.9}$$

Where $(.)^H$ denotes the Hermitian transpose.

Here $\boldsymbol{\psi}$ is a matrix of size $N \times M$ containing M features for each N sample

$$\boldsymbol{\psi} = \begin{bmatrix} \boldsymbol{\psi}(0) \\ \vdots \\ \boldsymbol{\psi}(N-1) \end{bmatrix} \tag{4.10}$$

and $\boldsymbol{y}$ is a vector of size $N \times 1$ containing the measured SI signal for N samples.

$$\boldsymbol{y} = \begin{bmatrix} y(0) \\ \vdots \\ y(N-1) \end{bmatrix} \tag{4.11}$$

The residuals are estimated using equation (4.12)

$$\boldsymbol{error} = \boldsymbol{y} - \boldsymbol{\psi}\hat{\boldsymbol{\theta}} \tag{4.12}$$

OLS is a non-adaptive method, meaning it can applied to the signal without computing any statistic. This can be seen in equation (4.9) where the whole signal is processed at the same time. This can be a weakness if the signal changes characteristics over time. However this leads to filtering using OLS having a low computational complexity.

4.3 Recursive Least Square

Recursive Least Square (RLS) algorithm is an adaptive version of the LS-algorithm presented in section 4.2. The system is modelled with features as shown in section 3, h is in the RLS algorithm the feature vector.

For initialization there are two main approaches. The first approach is the set $\hat{\boldsymbol{\theta}}[0] = \mathbf{0}$ and $\boldsymbol{P}[0] = \alpha\boldsymbol{I}$ where α is set to a large value. A good estimate for α is is the inverse of the estimate of the input power [34].

The other approach is to use a batch of the data to estimate $\boldsymbol{\theta}[p-1]$ and use RLS for $n \geq p$. Using this estimation, $\hat{\boldsymbol{\theta}}[p-1]$ uses weighted LS and P as a weighted covariance matrix. The weighted LS and weighted P can be described by equation (4.13).

$$\begin{aligned} \hat{\boldsymbol{\theta}}[p-1] &= (\boldsymbol{\psi}[p-1]^T\boldsymbol{W}[p-1]\boldsymbol{\psi}[p-1])^{-1}\boldsymbol{\psi}[p-1]^T\boldsymbol{W}[p-1]\boldsymbol{y}[p-1] \\ \boldsymbol{P}[p-1] &= (\boldsymbol{\psi}[p-1]^T\boldsymbol{W}[p-1]\boldsymbol{\psi}[p-1])^{-1} \end{aligned} \tag{4.13}$$

The algorithm follows a four step loop. The first step in equation (4.14) is to compute the Kalman gain.

$$K[n] = \frac{1}{\lambda + \boldsymbol{\psi}[n]^T\boldsymbol{P}[n-1]\boldsymbol{\psi}[n]}\boldsymbol{P}[n-1]\boldsymbol{\psi}[n] \tag{4.14}$$

The second step is to update the a priori error. Unlike LS which computes the current error, the a priori error is based off $\hat{\boldsymbol{\theta}}[n-1]$ as seen in equation (4.15)

$$\hat{e}[n] = y[n] - \boldsymbol{\psi}[n]^T\hat{\boldsymbol{\theta}}[n-1] \tag{4.15}$$

The third step is to update the weighted covariance matrix P described in equation (4.16).

$$\boldsymbol{P}[n] = \frac{1}{\lambda}(\boldsymbol{I} - \boldsymbol{K}[n]\boldsymbol{\psi}^T[n])\boldsymbol{P}[n-1] \tag{4.16}$$

Finally the weights are estimated using equation 4.17

$$\hat{\boldsymbol{\theta}}[n] = \hat{\boldsymbol{\theta}}[n-1] + K[n]\bar{e}[n] \tag{4.17}$$

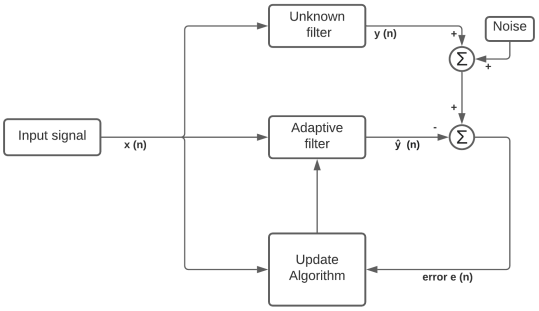

Figure 4.2: Block diagram of the RLS filter

The same procedure is showed in Figure 4.2 where the input signal x(n) goes through the unknown filter. The output from the unknown filter y(n) is filtered with the help of $y(\hat{n})$ which is a processed signal through the adaptive filter. The filter is also updated with the error e(n) which feedbacks through the update algorithm block and updates $y(\hat{n})$.

5 Results & Discussion

The following notations will be used throughout this section:

Tx_{in}	Input for transmitted signal
Tx_{out}	Output for transmitted signal
Rx	Received signal
$TxRx$	Tx_{out} plus Rx
$\hat{Rx}$	TxRx after cancellation

Table 5.1: Corresponding transmitted output power for given transmitted input power

Tx_{in} [dBm]	Tx_{out} [dBm]
5	3.7323
0	0.3896
-10	-9.8178

In table 5.1 the measured input of the transmitted signal Tx_{in} is given together with the power of the output of the transmitted signal Tx_{out}. The output of the transmitted signal is the power of the SI before digital cancellation in the receiver side whereas the input of the transmitted signal is in the transmitter side of the signal chain.

Table 5.2: Hyper parameters for the different models

Model	P_{order}	$memory$	P_{xterms}	$range_{xterms}$	$memory_{xterms}$
Linear	[1]	[10]	0	0	0
MP	[1 2 3 4 5 6 7 8]	[4 4 3 2 0 0 0 0]	0	0	0
GMP	[1 2 3 4 5 6 7 8]	[4 4 3 2 0 0 0 0]	[2 3]	[1 2]	[0 0]

In table 5.2 the chosen features for the linear, MP and GMP models are shown. The features are written as a vector where P_{order} is the order of the features and memory is how many memories that are used for the corresponding order. For example, if $P_{order} = [1, 3, 5]$ and $memory = [2, 1, 0]$ it means the features for the model consists of:

$$\boldsymbol{\psi}_1(t) = \begin{bmatrix} x(t)^1 \\ x(t-1)^1 \\ x(t-2)^1 \\ x(t)|x(t)|^2 \\ x(t-1)|x(t-1)|^2 \\ x(t)|x(t)|^4 \end{bmatrix} \tag{5.1}$$

The cross-terms, that are additional features for the GMP works in a similar way. P_{xterms} is the power for the crossterms. $memory_{xterms}$ is how much memory each crossterm order has and $range_{xterms}$ is how far back each memory crossterms.
For example: if $P_{xterms} = [3]$, $memory_{xterms} = [1]$ and $range_{xterms} = [2]$ the features would be,
For the lagging part:

$$\boldsymbol{\psi}_{lagging}(t) = \begin{bmatrix} x(t)|x(t-1)|^2 \\ x(t)|x(t-2)|^2 \\ x(t-1)|x(t-2)|^2 \\ x(t-1)|x(t-3)|^2 \end{bmatrix} \tag{5.2}$$

and for the leading part:

$$\boldsymbol{\psi}_{leading}(t) = \begin{bmatrix} x(t)|x(t+1)|^2 \\ x(t)|x(t+2)|^2 \\ x(t-1)|x(t)|^2 \\ x(t-1)|x(t+1)|^2 \end{bmatrix} \tag{5.3}$$

Equation (5.1), equation (5.2) and equation (5.4) combined gives the feature matrix as:

$$\boldsymbol{\psi}_{leading}(t) = \begin{bmatrix} \boldsymbol{\psi}_1(t) \\ \boldsymbol{\psi}_{lagging}(t) \\ \boldsymbol{\psi}_{leading}(t) \end{bmatrix} \tag{5.4}$$

The initial order hyperparameters guesses were based on the math of the features in the GMP described in section 2.4 and later optimized using trial and error. The memory hyperparameters were initially based on the AM/AM plots shown in section 2.4 and later trial and error. Finally the crosstermss were solely based on trial and error.

Table 5.3: BER achieved for different estimated SNR with 50Mhz bandwidth gray coded 4QAM for 7 different Rx powers.

Rx input power [dBm]	SNR [dB]	BER
-50	9.0305	0.0058
-45	13.9007	5.3538E-4
-40	18.8160	2.3005E-4
-35	23.9451	0
-30	29.0379	0
-25	34.0475	0
-20	39.0418	0

The SNR in Table 5.3 was calculated using equation (3.16), where the noise power is estimated through measurements during no transmission and assumed to have the same spectral density during transmission.

The BER was calculated using equation (3.15) where the total number of bits were a little over 3E+6.

Table 5.3 shows the bit error rate for different estimated signal to noise ratios, i.e. no interference. Since this thesis focus have been on self interference cancellation, there has been little focus on improving the BER but rather have a simple modulation and demodulation of the received signal. Table 5.3 is used as a lower bound of what could be achieved with SIC.

5.1 Full signal chain

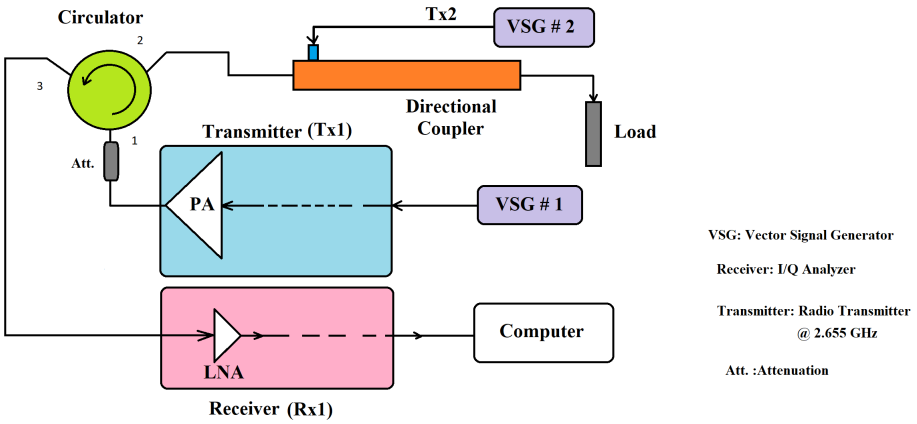

Figure 5.1: Measurement setup for full signal chain

For the simulation of the full signal chain two signals are generated. One signal that represents the transmitted signal and one signal that represents the received signal
The Transmitted signal is generated using a Vector Signal Generator (VSG). The signal passes through a power amplifier operating at 2.655 GHz with a 48 dBm nominal power. The amplified signal is directly attenuated by 40dB to not damage the equipment and also to represent the attenuation from the analog cancellation. The attenuated signal enters the circulator where the majority of the signal is sent towards the directional coupler that represents the antenna and into a load. Since the isolation in the circulator is not ideal SI leaks from the circulator to the receiver.
At the same time the received signal is generated using another VSG. The received signal goes through a directional coupler. The directional coupler represents the antenna and has a coupling factor of 16dB. The signal passes through the circulator and is added together with the SI. The combined received signal and SI passes through the Bandpass filter,is amplified using the LNA and downconverted before it goes through an additional lowpass filter and finally converted to a digital signal through the ADC. Finally the data is transferred to the computer. The whole procedure is explained in figure 5.1 with the equipment used presented in table 5.4

Table 5.4: Equipment used for full signal chain

Signal & Spectrum Analyzer	ROHDE & SCHWARZ FSW26
Vector Signal Generator	ROHDE & SCHWARZ SMW200A
Directional Coupler	Agilent 86205A (16 dB coupling)
Circulator	Molex UNH1023067/13
PA	Doherty LDMOS 2.655GHz 48dBm nominal power

The datasets provided contained data with Tx power = [5,4,3,2,1,0,-2,-4,-6,-8,-10] dBm to represent different number of non-linearities and Rx power ranges from -20 dBm to -50dBm measured every 5 dBm to represent different SNR (compared to the noise) and SINR (compared to the transmitted signal). For each combined Tx power and Rx power 20 different measurements were made to sum up to a total of over 3.5 megabits.

5.1.1 LS

The three different models in equation (5.5), (5.6) and (5.7) were created with the hyper-parameters of the feature matrix as shown in table 5.2 and the parameters $\hat{\boldsymbol{\theta}}$ was found with LS, as describe in section 4.2, on a training set of data. The features chosen in table 5.2 was found with trial and error, where for each case it was evaluated on an evaluation set data with MSE, the gain and by analyzing the spectrum of the residuals of Tx.

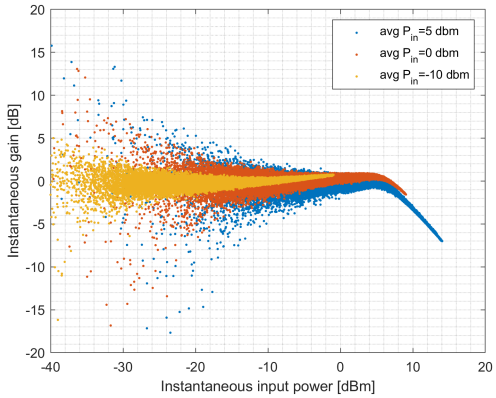

Figure 5.2: AM/AM plot for three Tx input power

$$X_{GMP}(n) = \boldsymbol{\psi}_{GMP}(n) * \hat{\boldsymbol{\theta}}_{GMP} \tag{5.5}$$

$$X_{MP}(n) = \boldsymbol{\psi}_{MP}(n) * \hat{\boldsymbol{\theta}}_{MP} \tag{5.6}$$

$$X_{Lin}(n) = \boldsymbol{\psi}_{Lin}(n) * \hat{\boldsymbol{\theta}}_{Lin} \tag{5.7}$$

$$Tx_{resid}(n) = Tx_{out}(n) - X_{model}(n) \tag{5.8}$$

The simulations were made with three different levels of average input power for Tx, -10dBm, 0dBm and 5dBm. The difference in input power results in a difference in the severity of nonlinearites. Figure 5.2 shows the nonlinearites for the different input powers. It can be seen that the PA behaves close to linear for an average input power of -10dBm (yellow). But for an average input power of 0dBm (orange) and 5dBm (blue) it shows a 1dB and 5dB compression respectively. The difference in nonlinear effect for different input power can also clearly be seen in figure 5.3 if Tx in (a), (b) and (c) are compared

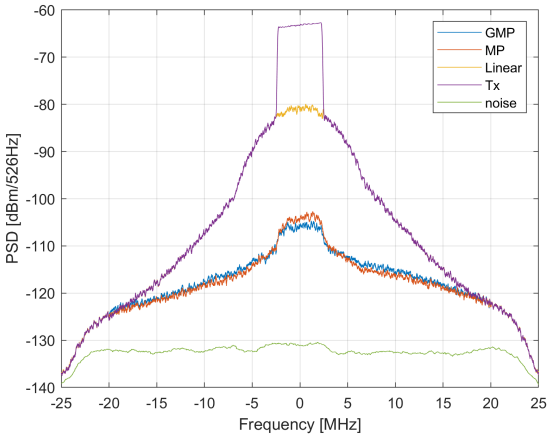

(a) $Tx_{out} = 3.7059dBm$

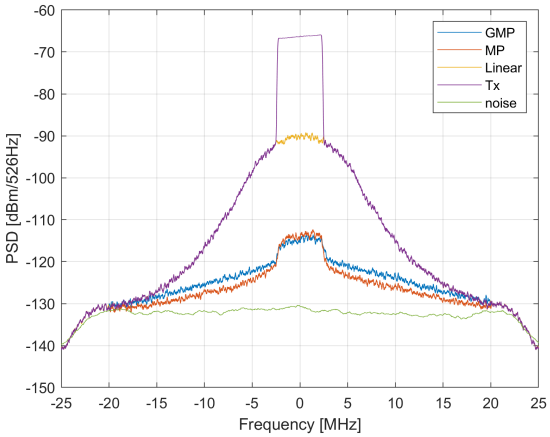

(b) $Tx_{out} = 0.3543dBm$

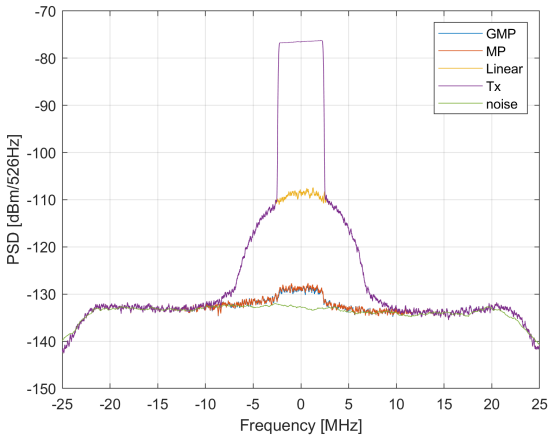

(c) $Tx_{out} = -9.756dBm$

Figure 5.3: PSD of residuals after DSIC using different using LS

The spectrum of the residuals from each model with features chosen as in table 5.2 can be seen in figure 5.3 (a), (b) and (c). Where (a) is strongly nonlinear, (b) is mildly nonlinear and (c) is weakly nonlinear. It can be clearly seen in all cases that with only linear cancellation the nonlinear residuals are present outside of the bandwidth but there is also nonlinear residuals withing the bandwidth. Both MP and GMP outperforms linear cancellation by around 20 dB for all the different levels of non-linearity.

As shown in table 5.2 the difference between MP and GMP are that there are cross-terms in GMP. In 5.3 (c) there is close to no benefit of the cross-terms, but in (a) the cross-terms in the GMP cancels about 3dB more than MP within the band. It can also be seen that the GMP performs worse than MP outside the bandwidth in (a) and especially in (b). However, since the interference is stronger within the bandwidth, further increasing cancellation within the bandwidth at the cost of decreasing the cancellation outside the bandwidth is still beneficial.

The MSE for each model and Tx power can be seen in table 5.5. The linear model is outperformed by both MP and GMP. For the strongly non-linear case the GMP performed better than the MP. However, for the weakly non-linear there is close to no difference in performance.

Table 5.5: Cancellation in dB within the bandwidth for linear model, MP model and GMP model at three Tx powers

	Tx power [dBm]		
model	3.71	0.35	-9.76
linear	17	24	32
MP	40	47	51
GMP	43	48	51

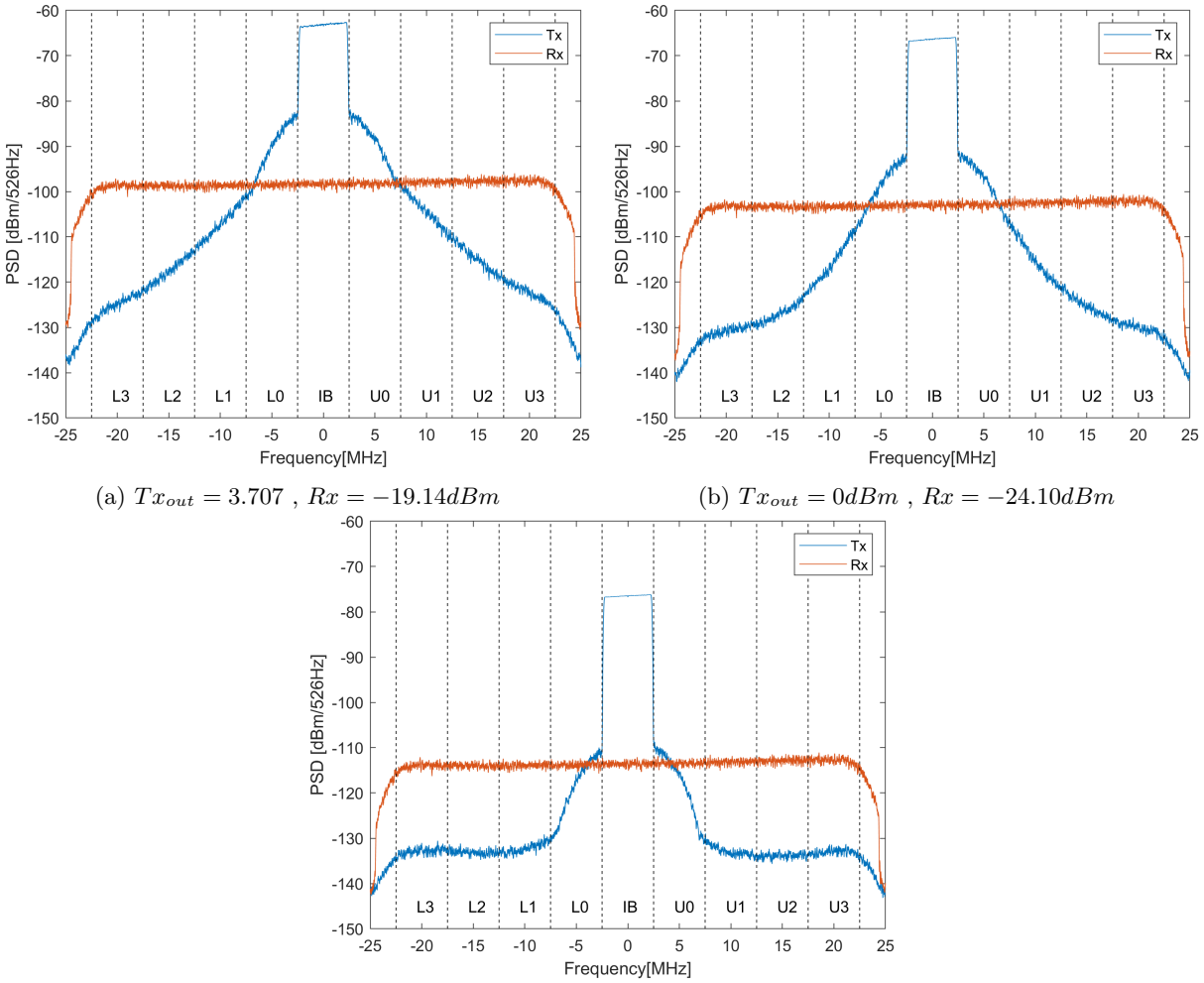

(a) $Tx_{out} = 3.707$, $Rx = -19.14dBm$

(b) $Tx_{out} = 0dBm$, $Rx = -24.10dBm$

(c) $Tx_{out} = -9.756$, $Rx = -34.03dBm$

Figure 5.4: PSD of interference signal Tx and desired signal Rx.

The cancellation of Tx was tested on a TxRx signal for the same Tx power as in figure 5.3 with a Rx power chosen at each case to keep the SINR within the band approximately the same for all Tx powers. As seen in figure 5.4 the Rx signal has a bandwidth of 50MHz and Tx a bandwidth of 5MHz. To see the nonlinear effects Tx has been divided into, within the band, adjacent channels and alternate channels as follows,

IB	Within the band $f \in [-2.5, 2.5]MHz$
$L0, U0$	Adjacent channel, lower and upper $f_L \in [-7.5, -2.5)MHz$ and $f_U \in (2.5, 7.5]MHz$
$L1, U1$	Alternate channel 1, lower and upper $f_L \in [-12.5, -7.5)MHz$ and $f_U \in (7.5, 12.5]MHz$
$L2, U2$	Alternate channel 2, lower and upper $f_L \in [-17.5, -12.5)MHz$ and $f_U \in (12.5, 17.5]MHz$
$L3, U3$	Alternate channel 3, lower and upper $f_L \in [-22.5, -17.5)MHz$ and $f_U \in (17.5, 22.5]MHz$

The estimated SINR for each channel was calculated with equation (3.17), which can be seen in figure 5.5. The difference in nonlinear effects can be clearly seen since the SINR is about -34dB within the band for (a),(b) and (c). For (c) there is close to no interference in the alternate channels, almost all interference is within the band and in the adjacent channels. But for (a) which is the most nonlinear, the non-linearity of Tx effects all the alternate channels and have a larger effect on the adjacent channels.

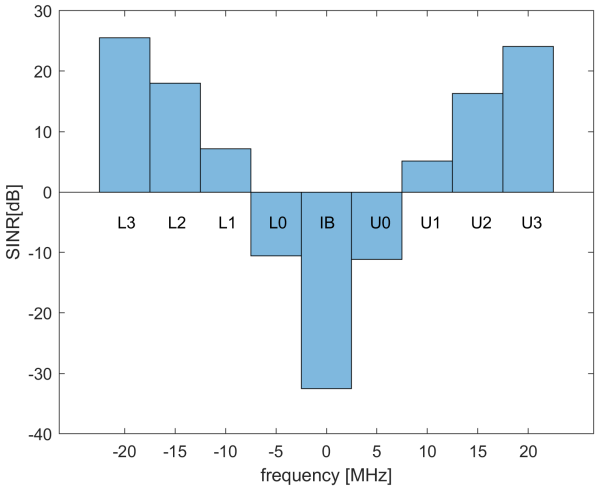

(a) $Tx_{out} = 3.707$, $Rx = -19.14dBm$

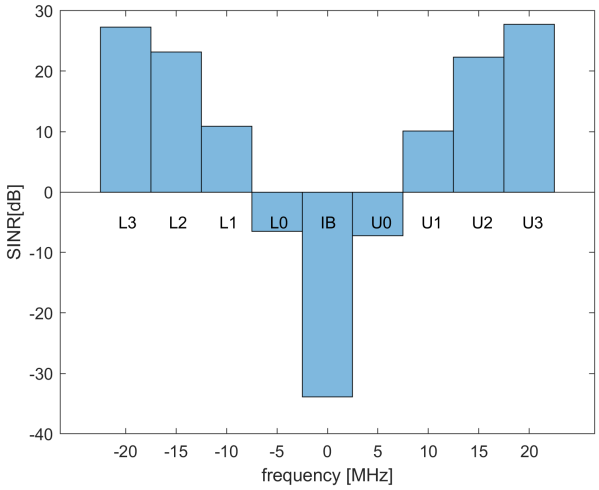

(b) $Tx_{out} = 0dBm$, $Rx = -24.10dBm$

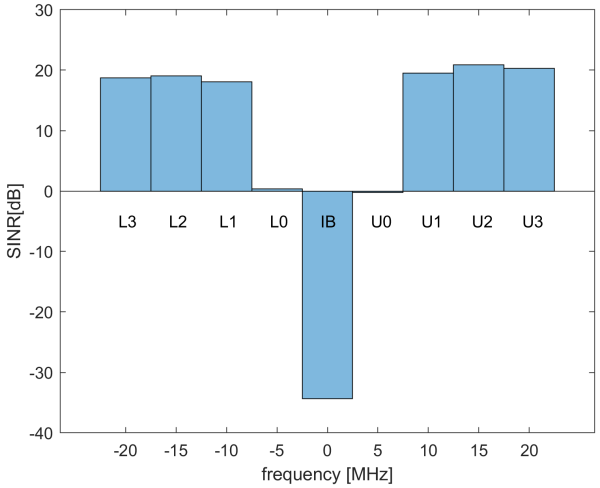

(c) $Tx_{out} = -9.756$, $Rx = -34.03dBm$

Figure 5.5: SINR before cancellation divided into in-band channel, adjacent channel (upper and lower), and three alternate channels at each side.

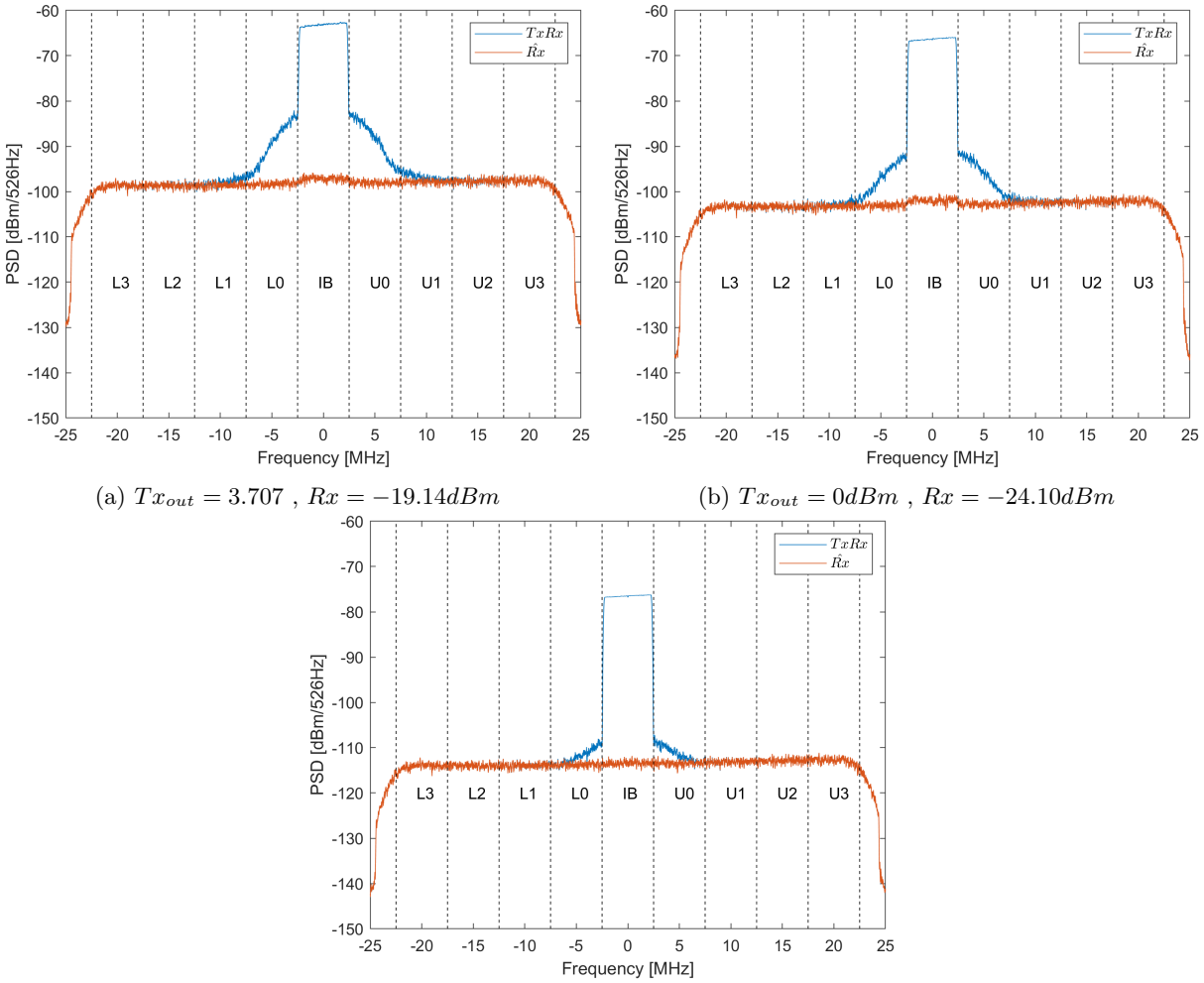

(a) $Tx_{out} = 3.707$, $Rx = -19.14dBm$

(b) $Tx_{out} = 0dBm$, $Rx = -24.10dBm$

(c) $Tx_{out} = -9.756$, $Rx = -34.03dBm$

Figure 5.6: PSD of Trx and $\hat{R}x$

Figure 5.6 shows the spectrum of TxRx, and Rx, where TxRx is a sum of the desired signal Rx and the transmitted signal Tx as

$$TxRx = Tx + Rx \tag{5.9}$$

and $\hat{R}x$ is the desired signal Rx plus the residuals of the cancellation of the transmitted signal Tx as

$$\hat{R}x = TxRx - X_{GMP} = Tx_{resid} + Rx \tag{5.10}$$

where X_{GMP} is the same as in equation (5.5).

In the PSD of $\hat{R}x$ (figure 5.6) the residuals of Tx are barely visible in (c) but in (a) and (b) it can be seen that there are residuals within the band. A better way of seeing the effects of the residuals of Tx is by looking at the estimated SINR divided into, within the band, adjacent channels and alternate channels as in figure 5.7. And also the BER of the demodulated $\hat{R}x$.

The SINR and the BER are closely related, i.e. lower SINR results in higher BER, which indicates that the desired signal Rx is not affected by the cancellation.

The results presented in figure 5.7 shows that the cancellation performs worse when Tx is more non-linear. Not only in the adjacent channels but also within the band. The numerical estimated SINR within the band of Tx before and after cancellation is shown in table 5.6 along with the BER. Where it can be seen that even though the SINR for Tx=-9.756dBm before cancellation is the worst, the cancellation performs best in this case which results in the best SINR after cancellation from the three cases. This result shows the importance of having a weakly nonlinear transmit signal to have better performance with FD.

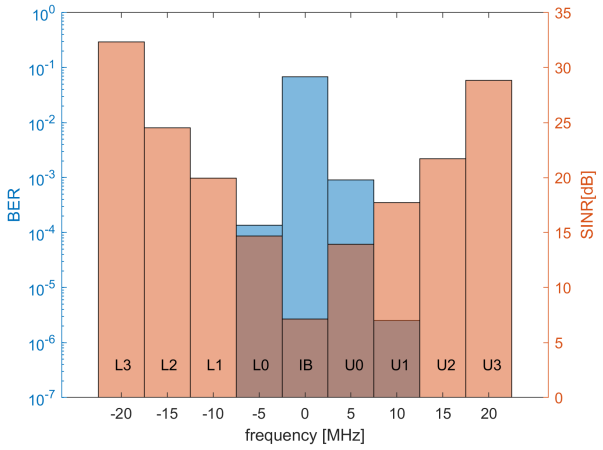

(a) $Tx_{out} = 3.707$, $Rx = -19.14dBm$

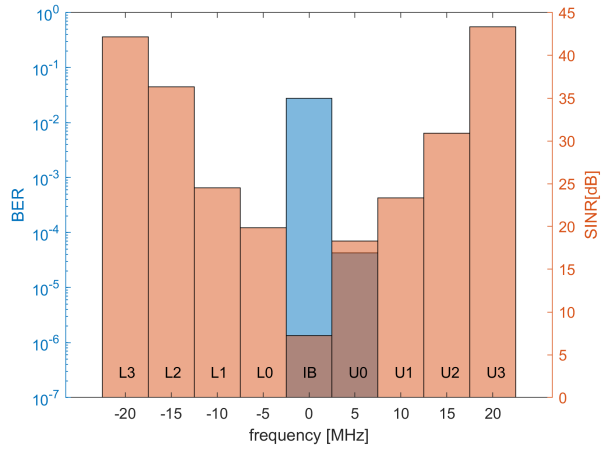

(b) $Tx_{out} = 0dBm$, $Rx = -24.10dBm$

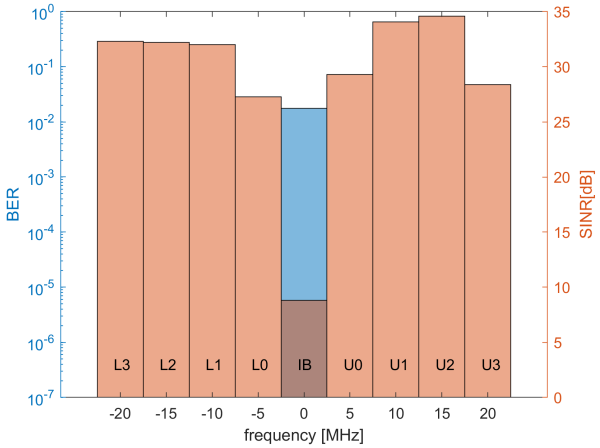

(c) $Tx_{out} = -9.756$, $Rx = -34.03dBm$

Figure 5.7: PSD of TxRx and $\hat{Rx}$

Table 5.6: SINR within the band

Tx power [dBm]	Rx power [dBm]	SINR before cancellation[dB]	SINR after cancellation[dB]	BER
3.707	-19.14	-32.55	7.13	6.83E-2
0.35	-24.10	-33.9	7.23	2.74E-2
-9.756	-34.03	-34.3	8.79	1.75E-2

To achieve a BER of 0 within the band the Rx power had to be increase by 10dB for the weakly nonlinear Tx

Table 5.7: SINR within the band when achieving a BER of 0

Tx power [dBm]	Rx power [dBm]	SINR before cancellation[dB]	SINR after cancellation[dB]	BER
-9.756	-24.0	-24	19	0

5.1.2 LMS

For LMS, the filter was trained one time for each Tx power to find an initial weight vector θ. The weights are found by using three different convergence factors (step-sizes) [39]. The convergence factors are split into a DC,linear and a non-linear part with $\beta_{DC} = [1e^{-7}]$, $\beta_{linear} = [0.2]$ and $\beta_{non-linear} = 1$.
The simulation is run with the initial weights as starting guesses and setting the convergence factor low to fine tune the filter. $\beta_{DC} = [1e^{-7}]$, $\beta_{linear} = [0.005]$ and $\beta_{non-linear} = 0.05$.

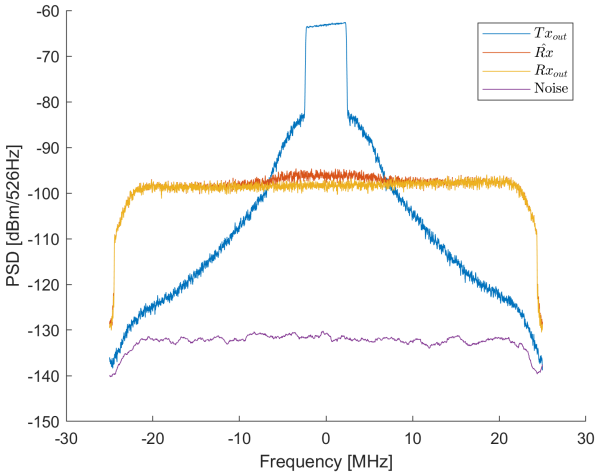

(a) PSD for $Tx_{out} = 3.707$, $Rx = -19.14dBm$

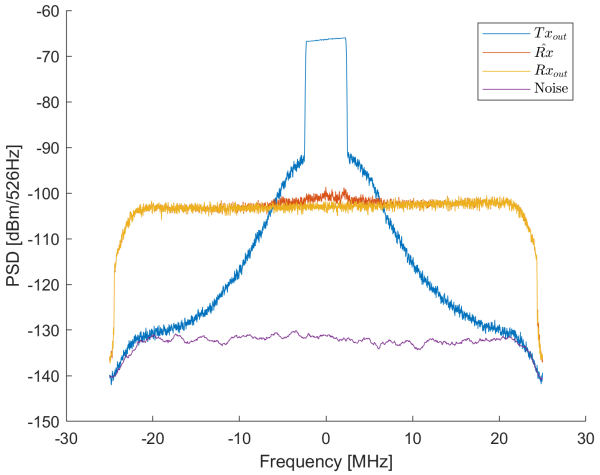

(b) PSD for $Tx_{out} = 0dBm$, $Rx = -24.10dBm$

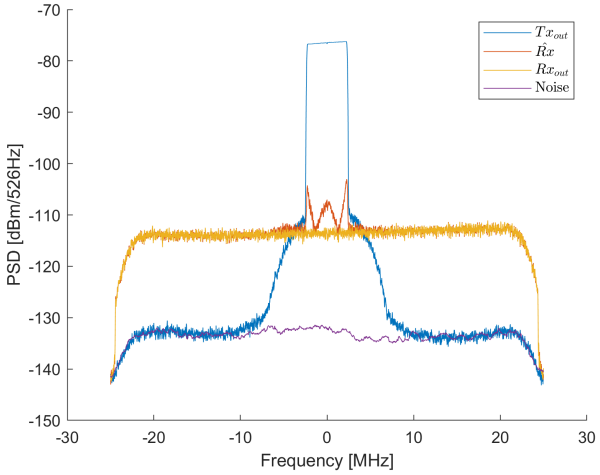

(c) PSD for $Tx_{out} = -9.756$, $Rx = -34.03dBm$

Figure 5.8: PSD using LMS where Tx_{out}, $\hat{Rx}$, Rx and measured noise floor is shown for different sets of Tx_{out} and Rx_{in}

Figure 5.8 presents the PSD of the cancellation using the NLMS algorithm. Figure 5.8a and 5.8b shows that the cancellation is not quite good enough to reach the desired level, however it can be seen that the step-size μ is at a stable size. In figure 5.8c it is clearly seen that all of the non-linearities are not cancelled out. This is due to LMS being a sensitive algorithm and it's hard to achieve good results with a fixed step-size independent of transmitted power.
It can also be noted that LMS are having trouble getting rid of some non-linearities that LS and RLS can deal with. It could possibly be that the reminding residuals could be cancelled if the step-size was fine-tuned further. Even though this was attempted, no success was found to achieve results for LMS as good as the results for RLS or LS.

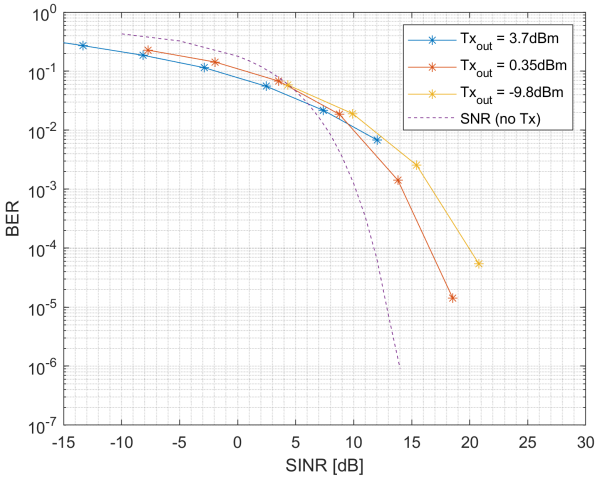

(a) SINR vs BER at the left side of Tx bandwidth

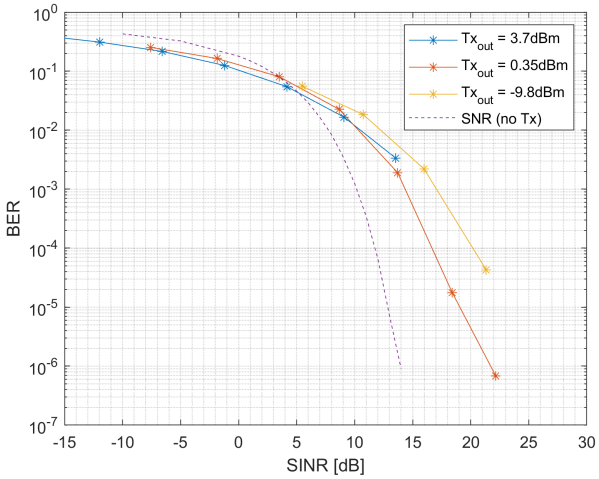

(b) SINR vs BER at the right side of Tx bandwidth

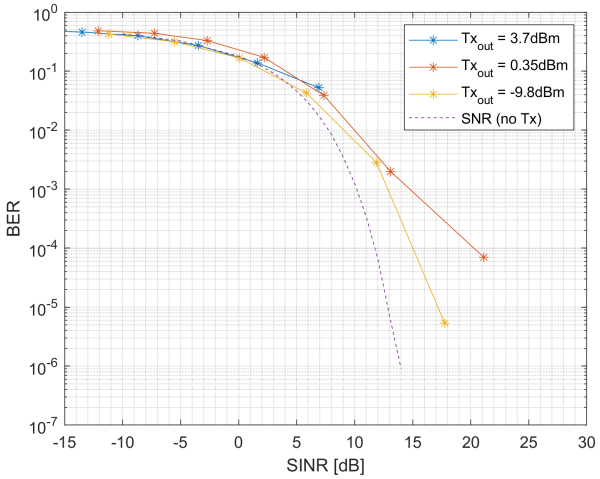

(c) SINR vs BER withing the bandwidth

Figure 5.9

Table 5.8

Rx	Tx input power [dBm]	BER LoB	BER In band	BER RoB
-34.03	-9.756	0.022	0.139	0.017
-24.10	0.354	0.001	0.039	0.002
-19.14	3.707	0.003	0.167	0.002

Table 5.9

Rx	Tx input power [dBm]	SINR compression[dB] LoB	SINR compression[dB] In band	SINR compression[dB] RoB
-34.03	-9.756	12.16	34.17	14.01
-24.10	0.354	14.51	41.25	14.62
-19.14	3.707	9.093	34.45	9.796

Figure 5.9 shows the differences for SINR vs BER within and outside of the bandwidth. In 5.9a and 5.9b it can be seen that outside of the bandwidth the BER vs SINR is a bit off compared to the theoretical value. This is a direct result of the power not being equally distributed over the designated bandwidth. As a result, the BER is better than the theoretical result at low SINR and worsens at higher SINR.
In Figure 5.9c which is within the band the theoretical values are closely followed for low SINR and

is just slightly off at higher SINR. This is because the cancellation is not the same for all frequencies resulting in various power at various frequencies. As the SINR is an estimated value within the band. The BER is slightly off compared to the theoretical values.
Another thing that can be seen is that for higher transmitted powers the value moves further away from the theoretical value for higher SINR. This is a as mentioned before, a result of the power amplifier introducing more non-linearities at higher transmitted powers.

This could further be seen in table 5.8 and 5.9 where it can be seen that the SINR compression is higher for transmitted power = 0. This is because the step-size was tuned in for especially for Tx = 0. Also the BER is significantly better for Tx = 0 than Tx = 5 and Tx = -10. Where the BER withing the band is very similar for the later two.
It could be possible to achieve even better result by improving the convergence factor μ further. This could be done by changing β which could've led to improved results. Although a significant increase in performance was seen when beta was changed from being a constant into a vector that had different values for DC,linear and non-linear parts. The results were still changing a lot for even small changes in β. This could also be improved further by using different beta for different transmitted power as there are different amount of non-linearities present in each case.

5.1.3 RLS

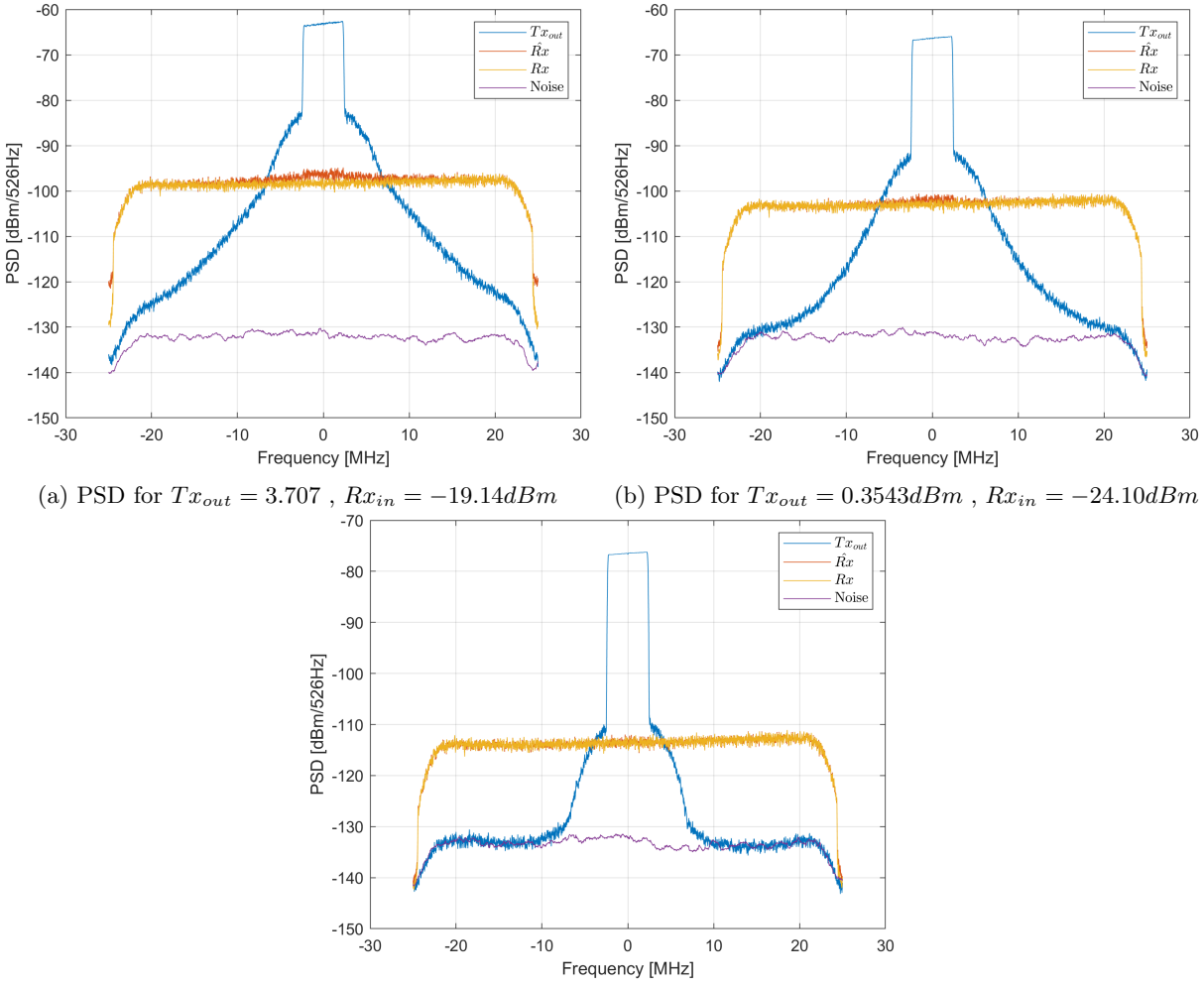

(a) PSD for $Tx_{out} = 3.707$, $Rx_{in} = -19.14dBm$

(b) PSD for $Tx_{out} = 0.3543dBm$, $Rx_{in} = -24.10dBm$

(c) PSD for $Tx_{out} = -9.756$, $Rx_{in} = -34.03dBm$

Figure 5.10: PSD using RLS where Tx_{out}, $\hat{Rx}$, Rx and measured noise floor is shown for different sets of Tx_{out} and Rx_{in}

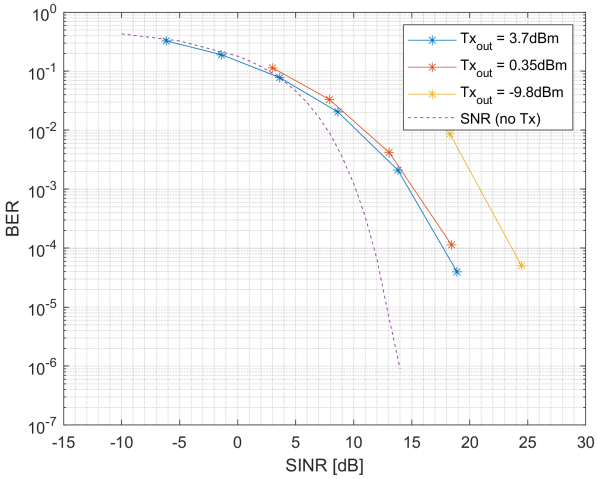

(a) SINR vs BER at the left side of Tx bandwidth

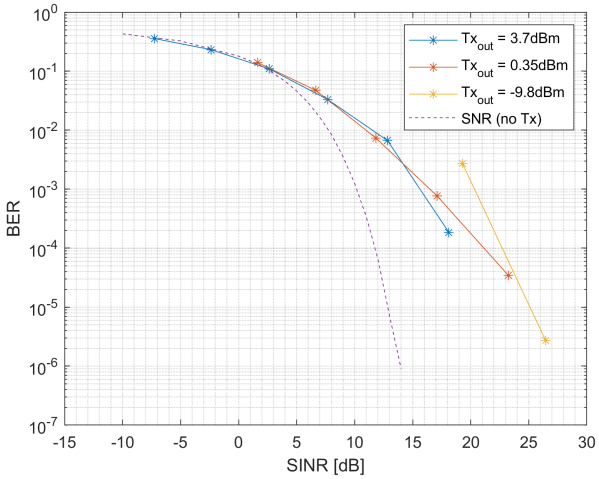

(b) SINR vs BER at the right side of Tx bandwidth

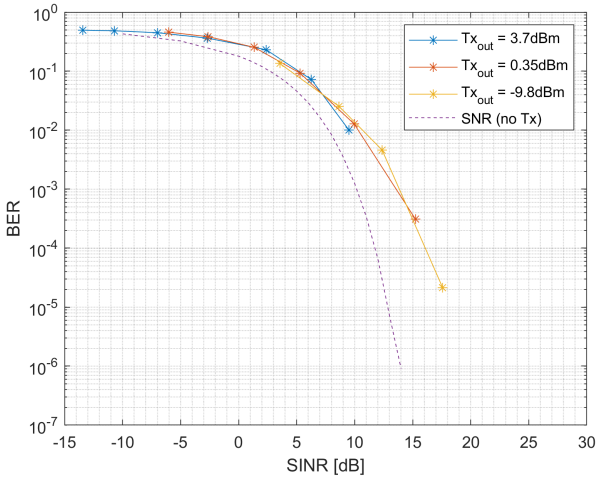

(c) SINR vs BER withing the bandwidth

Figure 5.11: SINR vs BER for LoB , In band and RoB using RLS algorithm

The BER vs SINR for left of band, right of band and in-band using RLS is presented in figure 5.11. The results for the out of band components can be a bit vague as the BER was zero for every measurement but 2. However the results are very similar independent of the transmitted power in comparison with the results from the LMS where they differed a bit more. This shows that the cancellation does not cancel the signal to a constant level but cancels different amount of power at different frequencies. The estimated SINR can therefore not be a sole representation of the result as it's not following the theoretical SNR vs BER curve for either of the methods. This basically mean that the residuals in this thesis can not be assumed to be noise, instead for a better evaluation of the method a combination of the SINR and the BER for each channel has to be estimated.

Table 5.10

Rx	Tx input power [dBm]	BER LoB	BER In band	BER RoB
-34.03	-9.756	0	0.005	0
-24.10	0.354	0	0.013	3.47E-5
-19.14	3.707	3.95E-5	0.072	1.85E-4

Table 5.11

Rx	Tx input power [dBm]	SINR compression[dB] LoB	SINR compression[dB] In band	SINR compression[dB] RoB
-34.03	-9.756	25.75	46.72	25.44
-24.10	0.354	25.11	43.85	24.15
-19.14	3.707	23.67	38.82	23.06

The tables 5.10 and 5.11 shows the corresponding results for the plots in figure 5.10 and 5.11. It can be noted that in this thesis the results for the RLS algorithm is better for lower transmitted power. The SINR compression is 8dB higher for Tx = -10 than Tx = 5. This corresponds to the BER that is shown in table 5.10 where the BER within the band is 0.5% for Tx = -10 whereas it is 7.2% for Tx = 5.
In the simulations LS and RLS shows a significantly better performance than LMS. This said, LMS could potentially be improved further by fine tuning the step-size even more. It can also be a bit misleading that LS and RLS shows similar results. As all of the measurements were made in a lab without environmental changes, the benefits of an adaptive filter never comes into action. If there were environmental changes the adaptive filters, both LMS and RLS, would probably be supreme to the non-adaptive LS filter.

It can also be noted that the result is dependent on the transmitted signal power. With increasing transmitted signal power there is increased disturbances in the form of non-linearities. This is further described in section 2.4. This can be handled with Digital Pre-Distortion techniques (DPD). The AM/AM of the signal for high transmitted signal power can be reduced to the characteristics of a transmitted signal with low signal power [41]. With the use of DPD, similar results could be achieved independent of the transmitted signal power.

6 Conclusion

Full duplex communication can transmit and receive signals simultaneously at the same frequency making it possible to double the spectral efficiency. Implementation of full duplex is difficult because of the self-interference, i.e. the transmitted signal that is leaked into the receiver. Because the transmitted signal is known it is theoretically possible to suppress the SI to the noise floor, however as the transfer function for the SI signal is not known this has to be approximated. In this thesis, three different methods of digital cancellation are presented together with an estimated model of the system. To estimate the transfer function of the SI signal the signal features were generated from three different functions.

1. A GMP to estimate the non-linearities and the cross terms of the signal chain.
2. The complex conjugates of all the features from the GMP to estimate the I/Q imbalance.
3. A DC feature to estimate a possible DC offset of the signal

It was also tested to model the system using a MP model and a linear model. It is worth noting that even though the presented results were done with the GMP the results of the simulation shows that at lower transmitted power (and less non-linearities) the MP model performs as well as the GMP with a lower computational complexity.

For LS, a one time training session on one signal was done to the weights of each corresponding feature. The weights together with their respective feature were used on several signals to estimate the cancellation and the BER. Different initial weights were found for different Tx power.
For RLS and LMS, a one time training session on one signal was done to estimate a starting point for the weights. The weights were then continuously updated as the signal was processed.

Different initial weights were found for different transmit powers. When the SIR between transmitted and received signal is the same, it was seen that the result improves with lower transmitted power. Higher transmitted power introduces more non-linearities, both within and outside of the band that is hard to model and therefore hard to cancel out. To achieve improved results with this methods, a better PA, better model or some kind of DPD would be necessary.

Even though the simulation shows a certain result the conditions include a lot of abnormalities compared to if the data came from an actual base station. This basically means that the results are not very reliable. Instead they would have to be tested in the right environment for a more precise validation.

With the given conditions the simulations indicate that LS and RLS outperforms LMS. The results shows a distinct difference in performance for RLS and LS compared to LMS. This said, LMS has a significantly lower computational complexity making it more suitable for implementation in full duplex systems. The trade-off between computational complexity and performance is tough.

The simulations indicate a strong correlation between performance and non-linearities especially for the LS and RLS algorithm. For RLS it was seen that the difference in BER could be up to 23% within the band, where the low Tx power had a BER of 0.5% and the high Tx power had a BER of 23%. These simulations were made with a similar SINR before cancellation. Although the SINR compression were 8dB higher for the latter the non-linearities introduced by the higher transmit power resulted in significantly worse BER. Simulations using the NLMS algorithm had a variable performance dependent on the step-size. Where a fine tuned step size increased the performance. In this thesis the NLMS algorithm showed a difference of up to 8dB in the SINR compression for a fixed step size. This corresponded to a BER drop from 14% down to 0.4%.

The LS algorithm simulations showed that with a SINR of -10dB before digital cancellation there is a BER of 10^{-3} in the adjacent channels. However this is for the worst case of the simulations and for SINR -5dB or higher the BER were close to zero.

The results shows indications that the GMP and MP performs similarly for weakly non-linear signals but for strongly non-linear signals GMP showed improved results. Both GMP and MP outperforms the linear model of the PA.

The data were measured in a lab environment. This means that the signals are very similar and without environmental changes. due to this, the benefits of adaptive filter are never really used. Therefore the measurements would have to be made in a better environment to properly see if these methods were good enough to be implemented in hardware. The simulation results of the LS filter is probably better than what it would actually be, especially if there were lots of changes in the environment.

7 Further work

One possible approach to improve the results would be to do piece-wise modeling for the GMP. It has been shown in [40] that dependent on the output power, different levels of non-linearities are present. It was shown that at higher output levels more non-linearities are present and that the signal is mainly linear at lower output powers. By distinguishing the different power levels and by using different number of non-linearities the signal could potentially be better modeled and the result improved.

It would also be very interesting to see if the results stays consistent if an actual antenna were used. This could introduce more disturbances on the signal and therefore worsen the results. If two antennas were used, different techniques such as beamforming and antenna polarization could be tested to see how that would affect the results.

Another idea would be to test the performance using neural networks with Adam optimizer as it has been tested by other researchers with promising results.

Appendix

Ls algorithm results

Table 7.1: Tx = 5dBm

Rx power	BER withing the band	BER outside the band	BER total	SINR [dB] before cancellaiton	SINR [dB] after cancellation
-20	0.0043	6.8129E-07	4.8066E-04	-17.9400	20.1855
-25	0.0679	1.0219E-04	0.0077	-22.9126	14.7130
-30	0.2141	0.0040	0.0276	-27.8853	9.6632
-35	0.3533	0.0264	0.0632	-32.8902	4.4325
-40	0.4418	0.0927	0.1320	-37.8862	-0.2705
-45	0.4836	0.2056	0.2369	-42.8960	-5.6331
-50	0.4955	0.3298	0.3484	-47.9014	-10.5077

Table 7.2: Tx = 0dBm

Rx power	BER withing the band	BER outside the band	BER total	SINR [dB] before cancellaiton	SINR [dB] after cancellation
-20	0	0	0	-15.0598	31.061
-25	1.5309e-04	0	1.7231E-05	-20.0699	23.6034
-30	0.0078	1.1923E-05	8.9361E-04	-25.0745	18.2026
-35	0.0890	3.0828E-04	0.0103	-30.0803	12.7205
-40	0.2438	0.0050	0.0319	-35.0887	7.7300
-45	0.3818	0.0355	0.0745	-40.1024	2.6713
-50	0.4588	0.1179	0.1562	-45.1367	-2.2684

Table 7.3: Tx = -10dBm

Rx power	BER withing the band	BER outside the band	BER total	SINR [dB] before cancellation	SINR [dB] after cancellation
-20	0	0	0	-4.6671	38.8844
-25	0	0	0	-9.6489	41.0233
-30	0	0	0	-14.6431	30.6355
-35	5.3717e-06	0	6.0461E-07	-19.6836	23.5132
-40	0.0016	0	1.7987E-04	-24.6601	18.1131
-45	0.0266	2.3164E-05	0.0030	-29.6708	12.6896
-50	0.1198	0.0052	0.0181	-34.6629	7.8331

References

[1] M. Gan et al., "Full Duplex for Next Generation of 802.11," 2019 IEEE 30th International Symposium on Personal, Indoor and Mobile Radio Communications (PIMRC Workshops), 2019, pp. 1-6, doi: 10.1109/PIMRCW.2019.8880844.

[2] M. Shammaa, H. Vogt, A. El-Mahdy and A. Sezgin, "Adaptive Self-Interference Cancellation for Full Duplex Systems with Auxiliary Receiver," 2019 International Conference on Advanced Communication Technologies and Networking (CommNet), 2019, pp. 1-8, doi: 10.1109/COMMNET.2019.8742358.

[3] B. van Liempd et al., "RF self-interference cancellation for full-duplex," 2014 9th International Conference on Cognitive Radio Oriented Wireless Networks and Communications (CROWNCOM), 2014, pp. 526-531, doi: 10.4108/icst.crowncom.2014.255756.

[4] M. S. Sim, K. S. Kim and C. Chae, "Self-Interference Cancellation for LTE-Compatible Full-Duplex Systems," 2018 IEEE International Conference on Communications Workshops (ICC Workshops), 2018, pp. 1-6, doi: 10.1109/ICCW.2018.8403641.

[5] A. Masmoudi and T. Le-Ngoc, "Self-Interference Cancellation Limits in Full-Duplex Communication Systems," 2016 IEEE Global Communications Conference (GLOBECOM), 2016, pp. 1-6, doi: 10.1109/GLOCOM.2016.7842258.

[6] F. J. Soriano-Irigaray, J. S. Fernandez-Prat, F. J. Lopez-Martinez, E. Martos-Naya, O. Cobos-Morales and J. T. Entrambasaguas, "Adaptive Self-Interference Cancellation for Full Duplex Radio: Analytical Model and Experimental Validation," in IEEE Access, vol. 6, pp. 65018-65026, 2018, doi: 10.1109/ACCESS.2018.2878448.

[7] Djemamar, Younes & Saida, Ibnyaich & Zeroual, Abdelouhab. (2015). Performance Analysis of QPSK, 4QAM, 16QAM and 64QAM with Binary and Gray Constellation Codes over AWGN Channel.

[8] A. Sahin, R. Yang, E. Bala, M. C. Beluri and R. L. Olesen, "Flexible DFT-S-OFDM: Solutions and Challenges," in IEEE Communications Magazine, vol. 54, no. 11, pp. 106-112, November 2016, doi: 10.1109/MCOM.2016.1600330CM.

[9] Andrea Goldsmith. 2005. Wireless Communications. Cambridge University Press, USA.

[10] Henrik Asplund, David Astely, Peter von Butovitsch, Thomas Chapman, Mattias Frenne, Farshid Ghasemzadeh, Måns Hagström, Billy Hogan, George Jöngren, Jonas Karlsson, Fredric Kronestedt, Erik Larsson, Chapter 8 - 3GPP Physical Layer Solutions for LTE and the Evolution Toward NR, Advanced Antenna Systems for 5G Network Deployments, Academic Press, 2020, Pages 301-350, ISBN 9780128200469, https://doi.org/10.1016/B978-0-12-820046-9.00008-3.

[11] 3GPP TS 25.101 v6.12.0 "User Equipment (UE) radio transmission and reception (FDD) Release 6", Section 6.2.2

[12] Dahlman, E., Parkvall, & Skold, J. (2016). 4G, LTE-advanced pro and the road to 5G (3rd ed.). San Diego, CA: Academic Press. Page 176-189

[13] Bob Witte, The basics of 5G's modulation, OFDM, April 16, 2020, `https://www.5gtechnologyworld.com/the-basics-of-5gs-modulation-ofdm/`

[14] Korpi D., Valkama M., Riihonen T. & Wichman R. (2013) Implementation challenges in full-duplex radio transceivers. In: Finnish URSI Convention on Radio Science

[15] D. Korpi, L. Anttila and M. Valkama, "Feasibility of in-band full-duplex radio transceivers with imperfect RF components: Analysis and enhanced cancellation algorithms," 2014 9th International Conference on Cognitive Radio Oriented Wireless Networks and Communications (CROWNCOM), 2014, pp. 532-538.

[16] Ghannouchi, F.M. & Hammi, Oualid & Helaoui, Mohamed. (2015). Behavioral Modeling and Predistortion of Wideband Wireless Transmitters.10.1002/9781119004424.

[17] William R. Deal, Vesna Radisic, Yongxi Qian, Tatsuo Itoh, 11 - Microwave Active Circuits and Integrated Antennas, Editor(s): WAI-KAI CHEN,The Electrical Engineering Handbook, Academic Press, 2005, Pages 691-706, 9780121709600, https://doi.org/10.1016/B978-012170960-0/50048-7.

[18] B. van Liempd et al., "RF self-interference cancellation for full-duplex," 2014 9th International Conference on Cognitive Radio Oriented Wireless Networks and Communications (CROWNCOM), Oulu, 2014, pp. 526-531, doi: 10.4108/icst.crowncom.2014.255756.

[19] Linyan Guo, Ming Deng, Qisheng Zhang, Xinyue Zhang, Zhenzhong Yuan, "Dual-Polarized On-Chip Antenna for 300 GHz Full-Duplex Communication System", International Journal of Antennas and Propagation, vol. 2017, Article ID 2837629, 7 pages, 2017. https://doi.org/10.1155/2017/2837629

[20] E. Everett, A. Sahai and A. Sabharwal, "Passive Self-Interference Suppression for Full-Duplex Infrastructure Nodes," in IEEE Transactions on Wireless Communications, vol. 13, no. 2, pp. 680-694, February 2014, doi: 10.1109/TWC.2013.010214.130226.

[21] M. B. Dastjerdi, T. Chen, N. Reiskarimian, G. Zussman and H. Krishnaswamy, "Self-interference cancellation via beamforming in an integrated full duplex circulator-receiver phased array," 2018 International Conference on Signal Processing and Communications (SPCOM), 2018, pp. 437-441, doi: 10.1109/SPCOM.2018.8724401.

[22] I. P. Roberts, J. G. Andrews, H. B. Jain and S. Vishwanath, "Millimeter-Wave Full Duplex Radios: New Challenges and Techniques," in IEEE Wireless Communications, vol. 28, no. 1, pp. 36-43, February 2021, doi: 10.1109/MWC.001.2000221.

[23] A. T. Le, L. C. Tran, X. Huang, Y. J. Guo and L. Hanzo, "Analog Least Mean Square Adaptive Filtering for Self-Interference Cancellation in Full Duplex Radios," in IEEE Wireless Communications, vol. 28, no. 1, pp. 12-18, February 2021, doi: 10.1109/MWC.001.2000210.

[24] B. Kaufman, J. Lilleberg, and B. Aazhang, "Analog baseband cancellation for full-duplex: An experiment driven analysis," arXiv preprint arXiv:1312.0522, 2013

[25] M. Yilan, O. Gurbuz and H. Ozkan, "Integrated Linear and Nonlinear Digital Cancellation for Full Duplex Communication," in IEEE Wireless Communications, vol. 28, no. 1, pp. 20-27, February 2021, doi: 10.1109/MWC.001.2000234.

[26] Chen, J. E. Modeling RF Systems. http://designersguide.org/Modeling/modeling-rf-systems.pdf

[27] F. Mkadem, A. Islam and S. Boumaiza, "Multi-Band Complexity-Reduced Generalized-Memory-Polynomial Power-Amplifier Digital Predistortion," in IEEE Transactions on Microwave Theory and Techniques, vol. 64, no. 6, pp. 1763-1774, June 2016, doi: 10.1109/TMTT.2016.2561279.

[28] D. R. Morgan, Z. Ma, J. Kim, M. G. Zierdt and J. Pastalan, "A Generalized Memory Polynomial Model for Digital Predistortion of RF Power Amplifiers," in IEEE Transactions on Signal Processing, vol. 54, no. 10, pp. 3852-3860, Oct. 2006, doi: 10.1109/TSP.2006.879264.

[29] D. R. Morgan, Z. Ma, J. Kim, M. G. Zierdt and J. Pastalan, "A Generalized Memory Polynomial Model for Digital Predistortion of RF Power Amplifiers," in IEEE Transactions on Signal Processing, vol. 54, no. 10, pp. 3852-3860, Oct. 2006, doi: 10.1109/TSP.2006.879264.

[30] `https://se.mathworks.com/help/signal/ref/designfilt.html`

[31] `https://community.sw.siemens.com/s/article/introduction-to-filters-fir-versus-iir`

[32] Steven W. Smith, CHAPTER 20 - Chebyshev Filters, Editor(s): Steven W. Smith, Digital Signal Processing, Newnes, 2003, Pages 333-342, ISBN 9780750674447, https://doi.org/10.1016/B978-0-7506-7444-7/50057-1.

[33] Marc T. Thompson, Chapter 14 - Analog Low-Pass Filters, Editor(s): Marc T. Thompson, Intuitive Analog Circuit Design (Second Edition), Newnes, 2014, Pages 531-583, ISBN 9780124058668, https://doi.org/10.1016/B978-0-12-405866-8.00014-0.

[34] Paolo S.R.Diniz., Adaptive Filtering - Algorithms and Practical Implementation (Fourth Edition).Chapter 11 - Nonlinear adaptive filtering, Page 470-480

[35] Kay, Steven M., Fundamentals of Statistical Signal Processing: Estimation Theory, Chapter 8 - Least Squares, Page 219-225

[36] M. Elsayed, A. A. A. El-Banna, O. A. Dobre, W. Shiu and P. Wang, "Low Complexity Neural Network Structures for Self-Interference Cancellation in Full-Duplex Radio," in IEEE Communications Letters, vol. 25, no. 1, pp. 181-185, Jan. 2021, doi: 10.1109/LCOMM.2020.3024063.

[37] D. Jorgesen. Iq, image reject, and single-sideband mixers. Technical report, Marki microwave, 2013.

[38] Concepts of Orthogonal Frequency Division Multiplexing (OFDM) and 802.11 WLAN `http://rfmw.em.keysight.com/wireless/helpfiles/89600b/webhelp/subsystems/wlan-ofdm/Content/ofdm_basicprinciplesoverview.htm`

[39] Paulo S. R. Diniz, 2013. Adaptive filtering. 4th ed.

[40] M. Alizadeh, P. Händel and D. Rönnow, "Basis Function Decomposition Approach in Piece-Wise Modeling for RF Power Amplifiers," 2018 26th Telecommunications Forum (TELFOR), 2018, pp. 1-4, doi: 10.1109/TELFOR.2018.8611865.

[41] Zhu, Anding & Draxler, Paul & Yan, Jonmei & Brazil, T.J. & Kimball, Donald & Asbeck, Peter. (2008). Open-Loop Digital Predistorter for RF Power Amplifiers Using Dynamic Deviation Reduction-Based Volterra Series. Microwave Theory and Techniques, IEEE Transactions on. 56. 1524 - 1534. 10.1109/TMTT.2008.925211.